



# Partial melting of zoisite eclogite from the Sanddal area, North-East Greenland Caledonides

Wentao Cao<sup>1,2</sup>, Jane A. Gilotti<sup>3</sup>, and Hans-Joachim Massonne<sup>4,5</sup>

<sup>1</sup>Department of Geology and Environmental Sciences,  
State University of New York at Fredonia, 230 Jewett Hall, Fredonia, NY 14063, USA

<sup>2</sup>State Key Laboratory of Geological Processes and Mining Resources,  
China University of Geosciences, 100083 Beijing, China

<sup>3</sup>Department of Earth and Environmental Sciences,  
University of Iowa, 115 Trowbridge Hall, Iowa City, IA 52242, USA

<sup>4</sup>Fakultät Chemie, Universität Stuttgart, Pfaffenwaldring 55, 70569 Stuttgart, Germany

<sup>5</sup>School of Earth Sciences,  
China University of Geosciences, 388 Lumo Road, Hongshan, 430074 Wuhan, China

**Correspondence:** Wentao Cao (cao@fredonia.edu)

Received: 14 November 2019 – Revised: 4 June 2020 – Accepted: 19 June 2020 – Published: 15 July 2020

**Abstract.** Metamorphic textures and a pressure–temperature ( $P$ – $T$ ) path of zoisite eclogite are presented to better understand the metamorphic evolution of the North-East Greenland eclogite province and this particular type of eclogite. The eclogite contained the mineral assemblage garnet, omphacite, kyanite, phengite, quartz and rutile at peak pressure. Partial melting occurred via breakdown of hydrous phases, paragonite, phengite and zoisite, based on (1) polymineralic inclusions of albite and K-feldspar with cusps into host garnet, (2) small euhedral garnet with straight boundaries against plagioclase, (3) cusps of plagioclase into surrounding phases (such as garnet), and (4) graphic intergrowth of plagioclase and amphibole next to anhedral zoisite grains. Isochemical phase equilibrium modeling of a melt-reintegrated composition, along with  $X_{\text{Na}}$ -in-omphacite and Si-in-phengite isopleths, yields a peak pressure of  $2.4 \pm 0.1$  GPa at  $830 \pm 30$  °C. A peak temperature of  $900 \pm 50$  °C at  $1.9 \pm 0.2$  GPa is determined using the rim composition of small euhedral garnet, as predicted by modeling a crystallized melt pocket. Zoisite growth at the expense of kyanite suggests that the  $P$ – $T$  path crossed the fields of zoisite growth at  $\sim 1.9$  GPa,  $800$ – $900$  °C on the modeled phase diagram of the bulk rock. A point on the exhumation path at  $\sim 1.3$  GPa and  $750$  °C is derived from hornblende-plagioclase thermometry and Al-in-hornblende barometry. The study demonstrates that paragonite, phengite and zoisite could contribute to partial melting of eclogite at near-peak  $P$  and during exhumation.

## 1 Introduction

Partial melting, along with subsequent melt extraction and magma ascent, leads to geochemical differentiation in large orogens (e.g., Clemens, 2006). The lower continental crust contains a significant portion of mafic rocks (Rudnick and Gao, 2014) and can undergo partial melting in eclogite facies when incorporated into large continental orogens. Investigating melting of eclogite from high-pressure (HP) terranes of large orogens is, therefore, critical to our understanding of geochemical differentiation processes. Despite retrograde

modification of melt-related textures, evidence of residual melt could be present along grain boundaries and as inclusions in porphyroblasts (Holness et al., 2011). Minerals crystallized from melt form low dihedral angles at silicate–melt contacts; for example, cusps of plagioclase that protrude into surrounding phases (e.g., omphacite) are interpreted to be crystallized melt (Cao et al., 2019; Wang et al., 2014). Melt can be captured during mineral growth and preserved as a crystallized assemblage in peritectic minerals such as garnet. For example, an inclusion assemblage of K-feldspar + quartz

± plagioclase ± calcite ± barite in garnet and omphacite in eclogite is interpreted as crystallized from melt that had formed by breakdown of hydrous minerals (e.g., Gao et al., 2014), such as phengite, paragonite and zoisite, on a retrograde path (Chen et al., 2014) or during burial (Massonne, 2011). Clinopyroxene + quartz ± kyanite ± plagioclase inclusions in garnet from an ultrahigh-pressure (UHP) eclogite from the North-East Greenland Caledonides are interpreted as crystallized melt formed from breakdown of an epidote-group mineral (Cao et al., 2019). Graphic intergrowths and peritectic minerals can also be present in partially melted eclogite. Once the melt mode reaches a certain threshold (Rosenberg and Handy, 2005), melt accumulates and channelizes, leading to melt loss from the source rock and formation of leucocratic layers. Thus, felsic veins, irregular patches and lenses, with a dacitic (e.g., Wang et al., 2014), granitic (e.g., Gilotti et al., 2014), tonalitic (e.g., Chen et al., 2010), and trondhjemitic (e.g., Labrousse et al., 2011) composition within eclogite bodies, are interpreted as crystallized melt derived from eclogite.

The North-East Greenland Eclogite Province (NEGEP; Gilotti, 1993), consisting of quartzofeldspathic gneisses that host eclogite and rare metapelite, is a large HP terrane that contains a small area of UHP rocks (Fig. 1; Gilotti and Ravna, 2002). Both eclogite and metapelite from the UHP terrane were partially melted (Lang and Gilotti, 2007, 2015; Cao et al., 2019). The UHP kyanite eclogite contains plagioclase cusps, polymineralic inclusions in garnet and omphacite, graphic intergrowths, and neoblasts, which are interpreted as evidence of partial melting (Cao et al., 2019). Experimental phase relations (Skjervlie and Patiño Douce, 2002) suggest that this eclogite was partially melted by breakdown of an epidote-group mineral on the exhumation path. An anatectic UHP metapelite contains leucocratic layers and polymineralic inclusions in garnet that are interpreted as crystallized pockets of melt derived from phengite breakdown (Lang and Gilotti, 2007). Gilotti et al. (2004) noted the presence of neosome along with web-like leucosome in zoisite eclogite (419655; Fig. 1c) from the HP terrane near Sanddal and suggested that the eclogite was partially melted. However, no systematic study has been conducted on partial melting of HP eclogites from this area.

In this work, we document textural evidence, infer a partial melting history and delineate a metamorphic  $P$ – $T$  path for zoisite eclogite from the Sanddal area (Fig. 1) in the NEGEP. Textures, such as plagioclase cusps, graphic intergrowths and polymineralic inclusions, are interpreted as formed from crystallized melt. Textures and phase equilibria indicate that paragonite, phengite and zoisite were the major reactants of the melt-producing reactions. Phase equilibrium modeling with a melt-reintegrated composition corroborates the former presence of paragonite, although it is not preserved in the mineral assemblage. Using mineral chemistry, textures, isopleth thermobarometry and Zr-in-rutile thermometry, a  $P$ – $T$  path is constructed from peak  $P$  of  $2.4 \pm 0.1$  GPa,  $830 \pm 30$  °C

to maximum  $T$  of  $900 \pm 50$  °C at  $1.9 \pm 0.2$  GPa in supra-solidus, and equilibrium reached at  $\sim 1.3$  GPa and 750 °C.

## 2 Geological setting

The North-East Greenland Eclogite Province covers an area of  $\sim 50\,000$  km<sup>2</sup> of eclogite-facies rocks (Fig. 1; Gilotti, 1993; Gilotti et al., 2008) on the northeastern margin of Laurentia. The NEGEP was formed in the overriding plate of Laurentia during the Caledonian continental collision with Baltica (Gilotti and McClelland, 2007; Gilotti and McClelland, 2011) and was thrust westward as the structurally highest sheet north of 76° N. The eclogite province is divided into three blocks – eastern, central, and western – by the NNW-striking Germania Land shear zone in the east (Hull and Gilotti, 1994; Sartini-Rideout et al., 2006) and the NNE-striking Storstrømmen shear zone in the west (Fig. 1b; Holdsworth and Strachan, 1991; Hallett et al., 2014). The NEGEP is mainly composed of quartzofeldspathic gneiss that contains layers and lenses of eclogitic rocks. Gneissic protoliths are Paleoproterozoic granodioritic rocks derived from 2.0 to 1.8 Ga juvenile calcalkaline arcs that were intruded by anorogenic granites at 1.75 Ga (Kalsbeek et al., 2008). The HP rocks include eclogite (*sensu stricto*), garnet clinopyroxenite, garnet websterite, websterite and coronitic metagabbro, the protoliths of which are mafic xenoliths in the Paleoproterozoic plutons, layered intrusions and late mafic dikes (Gilotti, 1993).

Peak metamorphic  $P$ – $T$  conditions and ages have been obtained from different parts of the NEGEP. Kyanite eclogites from Weinschenk Island in the central block yielded a minimum peak pressure around 1.8 GPa and a peak temperature of 850 °C (Elvevold and Gilotti, 2000). Eclogite and garnet websterite from the central block point to a peak  $P$ – $T$  range of 1.5–1.8 GPa, 750–780 °C (Brueckner et al., 1998) using the garnet-clinopyroxene Fe<sup>2+</sup>-Mg exchange thermometer (Ellis and Green, 1979), the albite to jadeite transformation barometer (Holland, 1980) and the Al-in-orthopyroxene barometer (Brey and Köhler, 1990; Harley and Green, 1982). Using the same thermometer and barometers, garnet websterite from the Danmarkshavn area in the central block returned a peak  $P$ – $T$  condition at 2.35 GPa and 790 °C (Brueckner et al., 1998). The HP metamorphism is approximately 420–395 Ma from U-Pb sensitive high-resolution ion microprobe (SHRIMP) dating of zircon and Sm-Nd mineral isochrons (Gilotti et al., 2004; Hallett et al., 2014; McClelland et al., 2016). Hallett et al. (2014) measured trace elements and dated zircon from zoisite eclogite 03-99, adjacent to the studied sample 03-59, with a SHRIMP reverse geometry instrument. The zircon has a low U and Th/U metamorphic rim around a higher U and Th/U core. Zircon cores of  $2010 \pm 10$  Ma give the age of the protolith. The rim shows a flat HREE (heavy rare earth elements) pattern and no Eu anomaly, typical of zircon crystallized in garnet-bearing

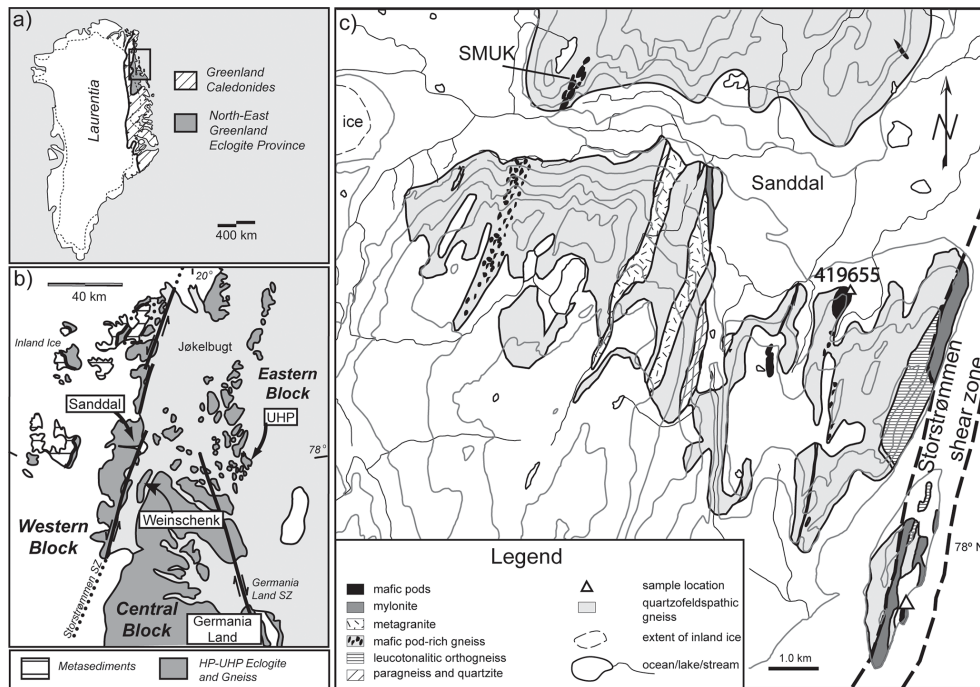


**Figure 1.** (a) Index map of the Greenland Caledonides showing the North-East Greenland Eclogite Province (NEGEP). (b) Geological map of the southern part of the NEGEP showing localities mentioned in the text. (c) Geological map of the Sanddal area (modified from Hallett et al., 2014) with the studied outcrop locality marked by a triangle in the Storstrømmen shear zone. Sample 419655 (triangle) refers to an eclogite studied by Gilotti et al. (2004). SMUK refers to Sanddal mafic–ultramafic complex.

eclogite-facies rocks (Rubatto, 2002), and yielded an age of  $394 \pm 12$  Ma, which is interpreted as the age of HP metamorphism.

An UHP terrane has been identified in the easternmost part of the hinterland on a small island at  $78^\circ$  N (Gilotti and Ravana, 2002). The regional extent of the UHP terrane is unknown, but it does not comprise the entire eastern block because HP eclogites are documented in Holm Land (McClelland et al., 2016). The UHP metamorphism is confirmed by coesite inclusions in zircon (McClelland et al., 2006). Peak  $P$ – $T$  conditions for the UHP terrane were estimated to be 3.6 GPa,  $970^\circ\text{C}$  by empirical thermobarometry (Gilotti and Ravana, 2002) and slightly lower at 3.4 GPa,  $940^\circ\text{C}$  using phase equilibrium modeling (Cao et al., 2019). The UHP metamorphism is 365–350 Ma or approximately 50 million years younger than the HP metamorphism (McClelland et al., 2006; Gilotti et al., 2014). U-Pb dating of later zircon domains reveals that partial melting started at 347 Ma and lasted until  $\approx 320$  Ma (Gilotti et al., 2014).

### 3 Outcrop and petrographic description

The Sanddal area is part of the western block of the NEGEP, which extends from the Storstrømmen shear zone (SSZ) to the inland ice. The SSZ is mainly composed of protomylonites to ultramylonites, with an exposed thickness of

$< 1$  km (Hallett et al., 2014; Hull and Gilotti, 1994). The area exposes mainly quartzofeldspathic gneisses with eclogitic pods, metagranite, orthogneiss, rare paragneiss and pegmatite (Hallett et al., 2014). Partially eclogitized, coronitic gabbro-norite pods occur in the Sanddal mafic–ultramafic complex (SMUK; Lang and Gilotti, 2001), which is located  $\sim 5$  km west of the SSZ (Fig. 1c).

The studied outcrop lies within the SSZ (UTM coordinates are zone 27  $\times$  VG 492 581, 8 657 828 m); Gilotti collected the samples in 2003. A 10 m long pod with well-preserved eclogite enclosed in quartzofeldspathic protomylonite (Fig. 2a–d) was selected for this study. The eclogitic pod is heterogeneous (Fig. 2a–d). The inner part is massive and mainly consists of garnet-rich restite, with bimineralic eclogite, quartz eclogite and zoisite eclogite, whereas outer parts display a strong gneissosity to mylonitic foliation in dominantly zoisite-rich gneiss. We focus on two samples, 03-57 and 03-59, that are remarkably well preserved in a low-strain boudin, despite their location in a shear zone; the two samples are representative of the inner and outer parts of the eclogite pod, respectively. Leucocratic veins, both concordant and discordant and up to 5 cm thick, in the eclogite pods (Fig. 2a–d) are mainly composed of plagioclase, quartz and amphibole. A leucotonalitic orthogneiss is located just west of the pod and extends discontinuously for 3 km along the SSZ (Fig. 1c).

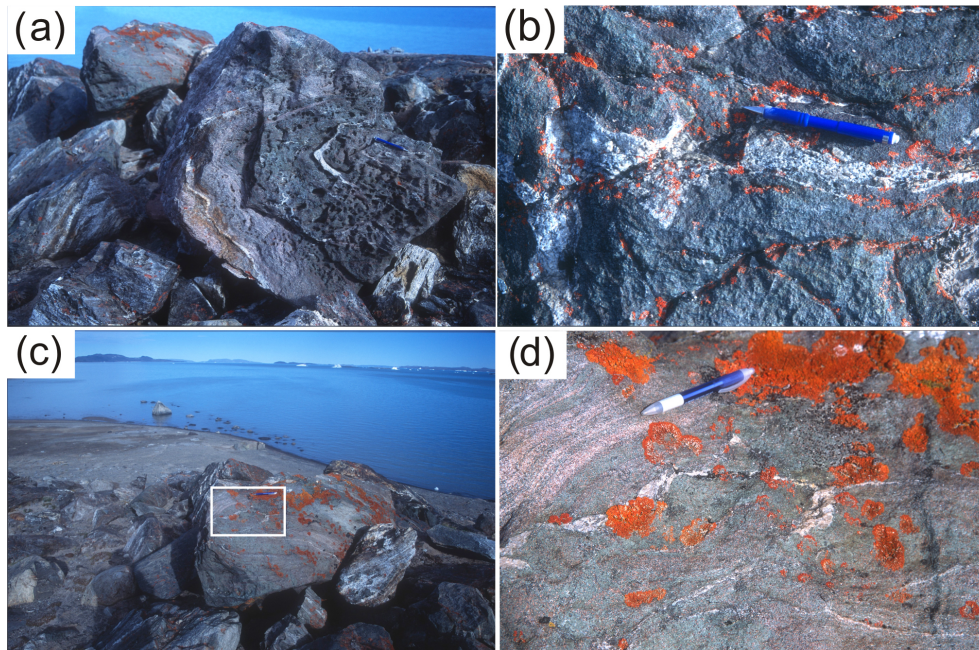


**Figure 2.** Photographs of the studied outcrop from the Storstrømmen shear zone near Sanddal. The orange color is lichen; pencil for scale. (a) Eclogite pod with leucocratic veinlets surrounded by foliated zoisite eclogite and quartzofeldspathic gneiss. (b) Felsic veinlets in the center of the eclogite pod. (c) Eclogite pod with felsic veins surrounded by foliated zoisite eclogite. The white box marks the position of (d). (d) Close-up of internally derived felsic vein in eclogite and connection with felsic zoisite eclogite.

Modes were determined using PetrogLite™ point-counting software with an automated Petrog™ stepping stage at the Department of Earth and Environmental Sciences, University of Iowa. A total of 200 points were counted per thin section. Metamorphic assemblages and melt-related textures are described for the two eclogite samples and then used for deciphering the metamorphic evolution.

### 3.1 Zoisite eclogite 03-57

The sample is a partially retrogressed zoisite eclogite collected from the inner part of the mafic pod. Mineral modes (in vol. %) are 11 % garnet, 16 % omphacite and diopside, 29 % amphibole, 18 % plagioclase, 4 % kyanite, 14 % diopside-plagioclase-amphibole symplectite, 5 % quartz, 3 % zoisite, and accessory biotite and rutile. The eclogite is weakly foliated with millimeter-thick plagioclase and quartz layers comprising 10 %–15 % of the whole rock. Figures 3a–d and 4 show the representative textures in the eclogite.

Two generations of garnet, larger (Grt I) and smaller (Grt II), are present. Large garnet (Grt I), up to centimeter sized, is anhedral with embayed grain boundaries, and rarely displays straight boundaries against plagioclase (Figs. 3a and 5). Abundant inclusions are present in the core of Grt I, with fewer inclusions in the rim. The inclusions are monomineralic omphacite, kyanite, plagioclase, K-feldspar, albite, zoisite, quartz and rutile, as well as polymineralic inclusions (Fig. 4a–d). Polymineralic inclusions are dominated by K-

feldspar ± albite ± kyanite ± phengite ± apatite (Fig. 4a, b), while polymineralic inclusions of phengite + kyanite, K-feldspar + allanite and K-feldspar + albite + zoisite are present in the inner rim. The K-feldspar + albite inclusions display cusps into each other (Fig. 4b, f) and into Grt I (Fig. 4e, f). Fractures in the large garnet are filled by the same mineral assemblage as the connected polymineralic inclusions (Fig. 4b). Small euhedral Grt II, about 200 μm in diameter, contains few inclusions and straight boundaries against plagioclase (Fig. 3a).

The matrix is mainly composed of clinopyroxene, kyanite, amphibole, zoisite, biotite, plagioclase and K-feldspar. Matrix kyanite, subhedral in shape, is commonly rimmed by subhedral to anhedral zoisite (Fig. 4a). Phengite is only present as inclusions in garnet (Fig. 5), but minor biotite clusters in the matrix indicate the former presence of phengite at peak pressure. Diopside plus plagioclase and amphibole forms symplectite around omphacite. The width of the symplectite lamellae varies from 5 to 50 μm (Fig. 3c). Amphibole is anhedral or poikiloblastic. The anhedral amphibole is blocky and large (up to 800 μm), replacing Grt I with plagioclase. The poikiloblastic amphibole is intergrown with plagioclase, which displays cusps pointing into amphibole. Graphic intergrowth of amphibole and plagioclase is observed locally in the matrix, adjacent to anhedral zoisite (Fig. 3b–c), forming millimeter-long channel-like features. Zoisite surrounds subhedral to anhedral up to millimeter-sized kyanite and is anhedral to subhedral adjacent to pla-

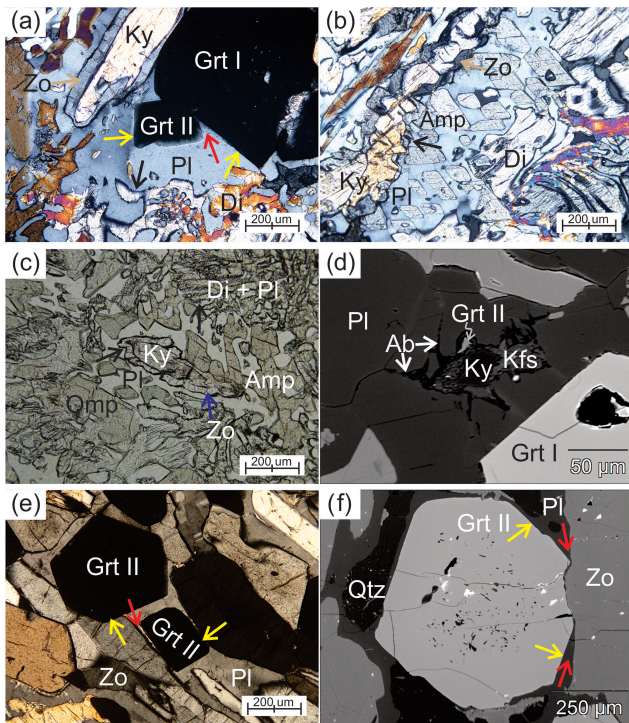


**Figure 3.** Photomicrographs of representative textures: (a–d) are from sample 03-57 and (e–f) are from 03-59. Red arrows mark interstitial plagioclase into garnet–garnet or garnet–zoisite boundary. Yellow arrows point to euhedral garnet against plagioclase. Black arrows mark embayed boundaries of clinopyroxene or zoisite. (a) Small euhedral garnet (Grt II) growing on large garnet (Grt I), both show a euhedral face against plagioclase. Garnet grains are adjacent to subhedral zoisite surrounding kyanite and anhedral diopside (cross-polarized light, XPL). (b) Graphical intergrowth of amphibole and plagioclase next to anhedral diopside and kyanite, which is surrounded by anhedral zoisite. Note that the amphibole grains have the same crystallographic orientation (XPL). (c) Kyanite surrounded by anhedral zoisite, which is next to poikiloblastic plagioclase. The plagioclase displays cusps into diopside and zoisite (plane-polarized light, PPL). (d) Backscattered electron (BSE) image showing polymineralic inclusions in plagioclase adjacent to Grt I with euhedral crystal faces. The polymineralic inclusions of kyanite + K-feldspar + albite + Grt II show sharp offshoots into plagioclase. (e) Euhedral Grt II, zoisite, omphacite and plagioclase. Plagioclase shows cusps into Grt II–zoisite boundaries (XPL). (f) Photomicrograph showing Grt II with a euhedral crystal face against plagioclase adjacent to zoisite. Inclusions are common in the core and rare in the rim.

gioclase (Fig. 3a–c). Plagioclase occurs in the symplectite and the matrix and forms cusps into anhedral clinopyroxene (Fig. 3a–c). Matrix plagioclase (Fig. 3d) adjacent to an euhedral crystal face of Grt I contains a polymineralic inclusion of garnet + kyanite + K-feldspar + albite. Kyanite in the inclusion is rimmed by K-feldspar and in turn surrounded by albite; the albite displays sharp offshoots into the host plagioclase. Cusps of plagioclase into clinopyroxene, amphibole,

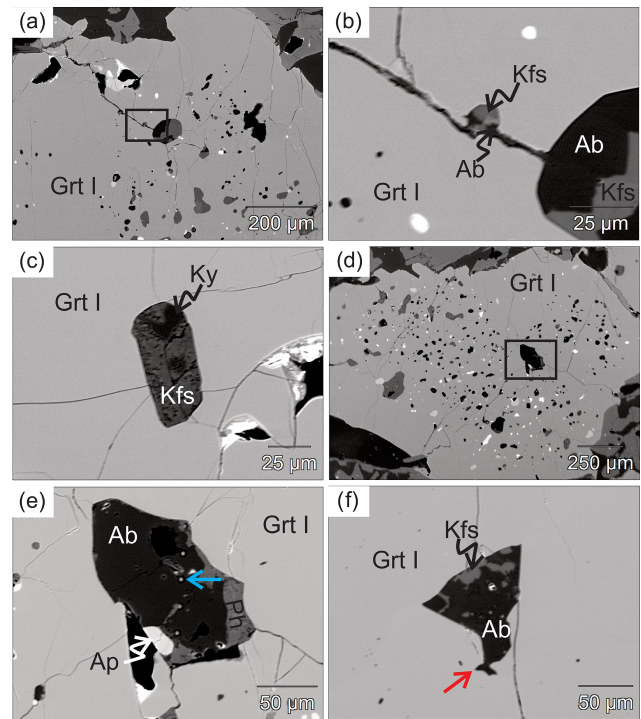


**Figure 4.** BSE images of inclusions in eclogite 03-57. (a) Porphyroblastic garnet (Grt I) with abundant polymineralic inclusions and fractures. The black box shows the position of (b). (b) Polymineralic inclusions of albite and K-feldspar along with cracks that are filled with the same mineral assemblage. (c) Polymineralic inclusions of K-feldspar and kyanite in Grt I. (d) Garnet I contains numerous poly- and monomineralic inclusions. The black box shows the position of (e). (e) Polymineralic inclusions of albite, apatite and phengite. The five equally spaced bright spots (blue arrow) on the polymineralic inclusions are caused by a line scan of garnet (Grt I) during analysis. (f) Polymineralic inclusion of albite and K-feldspar in Grt I. Note the cusped contact marked by the red arrow.

zoisite and garnet–garnet boundaries are also observed in the matrix (Fig. 3a–c). Rare brown biotite, either in the matrix or enclosed in zoisite, coexists with plagioclase, kyanite and Grt II.

These textures suggest that the peak pressure assemblage is Grt I, omphacite, kyanite, phengite, quartz and rutile (Figs. 3 and 4; Table 2), while the lower-pressure assemblage contains Grt II and polymineralic inclusions (e.g., with the presence of K-feldspar and/or albite) in the core and inner rim of Grt I, diopside, kyanite, zoisite, amphibole, plagioclase and minor biotite (Fig. 3a–d; Table 2). Polymineralic inclusions and fractures within garnet suggest that the inclusions are crystallized melt.

### 3.2 Zoisite eclogite 03-59

Sample 03-59 is a zoisite eclogite collected from the foliated margin of the eclogite pod. A strong foliation is defined by millimeter-thick leucocratic layers alternating with zoisite-

**Table 1.** Assemblage and textural settings of minerals from the studied samples. Abbreviations for the textural relation are as follows: pb, porphyroblast; pbt, poikiloblast; m, matrix; i, inclusion; s, symplectite; r, retrograde mineral; a, accessory. Abbreviations for minerals are as follows: Cpx, clinopyroxene including omphacite and diopside; Amp, amphibole; Ph, phengite; other mineral abbreviations follow Kretz (1983).

Sample	Grt	Cpx	Ky	Amp	Zo	Ph	Bt	Pl	Kfs	Qtz	Rt	Ap	Ttn	Zrn	Opaque
03-57	pb	m/i/s	m/i	m/s	m/i	i	m/i/r	pbt/m/i/s	m/i	i	m/i	a	a	a	a
03-59	pb	m/s	m/i	m/s	pb/m	i (?)	s/r	m/s	m	m/i	m/i	a		a	a

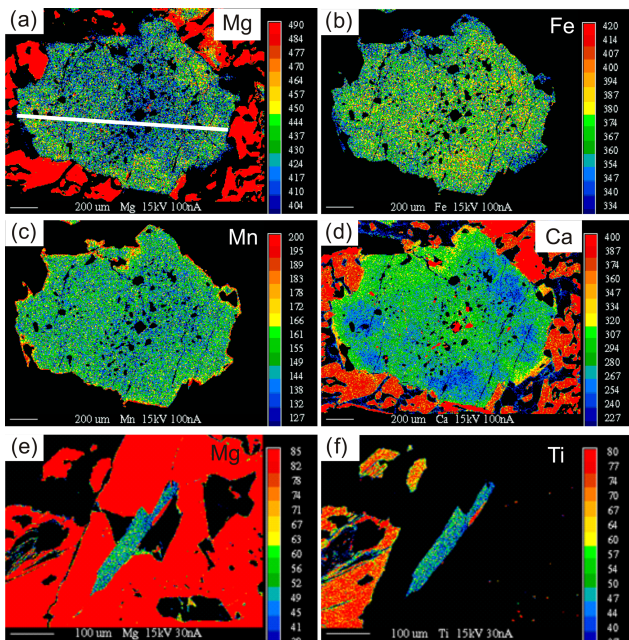


**Figure 5.** X-ray maps showing compositional zoning of garnet (a–d) and phengite (e–f) in zoisite-eclogite 03-57. The garnet displays a relatively homogeneous core, which contains numerous inclusions and a zoned inner rim and outer rim. The inner rim of the garnet contains few inclusions and displays patchy zoning in Mg and Ca. The garnet outermost rims are richer in Fe, Ca and Mn. (e–f) Phengite shows slight variation of Mg and thus Si and Ti.

rich layers. The peak mineral assemblage is similar to that in sample 03-57, i.e., garnet, omphacite, kyanite, zoisite, phengite, quartz and rutile. A distinctive feature is the very high abundance of zoisite (36 %) oriented sub-parallel to the major foliation. Zoisite occurs as euhedral to subhedral crystals up to 1 cm long (Fig. 3e). Textures of the peak assemblage differ from sample 03-57: Grt II (9 %) is small (< 1 mm), euhedral to subhedral (Fig. 3e), with polymineralic inclusions of plagioclase, kyanite, quartz and phengite (?) common in the core and rare in the rim (Fig. 3f). Matrix kyanite (7 %) is subhedral and commonly enclosed by zoisite and plagioclase. Subhedral to anhedral clinopyroxene (8 %) in the matrix typically shows sharp embayments by plagioclase. Accessory rutile and zircon are present as inclusions and matrix minerals. The sample is strongly laminated with leucocratic

**Table 2.** Developmental sequence of the metamorphic minerals in matrix of the studied samples: phengite and zoisite in the matrix and phengite and paragonite in garnet broke down during partial melting. The dashed line indicates inferred presence of mineral.

	Prograde	Peak P	Melting	Crystallization	Retrograde
Garnet	—————	—————	—————	—————	—————
Clinopyroxene	—————	—————	—————	—————	—————
Kyanite	—————	—————	—————	—————	—————
Zoisite	—————	—————	—————	—————	—————
Amphibole	—————	—————	—————	—————	—————
Phengite	—————	—————	—————	—————	—————
Paragonite	-----	-----	-----	-----	-----
Biotite	—————	—————	—————	—————	—————
K-feldspar	—————	—————	—————	—————	—————
Plagioclase	-----	-----	-----	-----	-----
Quartz	—————	—————	—————	—————	—————
Rutile	—————	—————	—————	—————	—————

layers of various thickness (up to 5 mm) composed of plagioclase, large quartz grains, minor small euhedral garnet and anhedral clinopyroxene. Omphacite is partially replaced by symplectitic intergrowths of diopside and plagioclase with or without amphibole. Diopside rims adjacent to the leucosomes typically show sharp embayments by plagioclase or quartz. Poikiloblastic plagioclase (17 %) forms cusps into subhedral to anhedral amphibole (15 %) and Grt II-zoisite (Fig. 3e, f) and typically surrounds anhedral kyanite. Minor biotite (~ 1 %) coexists with plagioclase in the leucocratic layers.

## 4 Mineral chemistry

### 4.1 Analytical conditions

Major element composition of minerals was determined using a Cameca SX-100 electron microprobe (EMP) equipped with five wavelength-dispersive spectrometers at the Institut für Mineralogie und Kristallchemie, Universität Stuttgart, Germany. Natural albite, orthoclase, diopside, and rhodonite and synthetic hematite, periclase, BaSO<sub>4</sub>, TiO<sub>2</sub>, Cr<sub>2</sub>O<sub>3</sub>, and Al<sub>2</sub>O<sub>3</sub> were used as standards. X-ray maps of garnet were

obtained with operational conditions of 15 kV accelerating voltage, 100 nA beam current and 70 ms pixel time with step sizes from 6 to 8  $\mu\text{m}$ . Phengite was mapped using 15 kV accelerating voltage and 30 nA beam current with 3  $\mu\text{m}$  step size. Points were analyzed with 15 kV accelerating voltage for all minerals, and 15 nA beam current for garnet and kyanite and 10 nA for all other minerals except rutile. Counting time was 20 s for peak and background analysis.

Point analysis of rutile was performed with 15 kV accelerating voltage and 90 nA beam current with a focused beam. To monitor the possible influence of surrounding silicate minerals, Si was also measured. The peak and background counting times for Zr, Cr, Fe, Nb and Si were set at 100 s. Wollastonite, J43\_Zir,  $\text{Cr}_2\text{O}_3$ ,  $\text{Fe}_2\text{O}_3$  and Nb were used as standards.

The PAP correction procedure by Cameca was used to correct raw counts. Chemical composition was calculated with Excel spreadsheet CALCMIN (Brandelik, 2009) for all minerals except amphibole for which the Excel spreadsheet by Locock (2014) was used, following the nomenclature of Hawthorne et al. (2012). Ferric iron ( $\text{Fe}^{3+}$ ) is calculated for all minerals. Calculated mineral formulae are presented in Tables 3–6.

## 4.2 Analytical results

### 4.2.1 Zoisite eclogite 03-57

Garnet I displays slight and patchy zoning (Fig. 5a–d; Table 3). The core is composed of 40 mol % almandine, 34 mol % pyrope, 24 mol % grossular (+andradite) and 1 mol % spessartine ( $\text{Alm}_{40}\text{Prp}_{34}\text{Grs}_{24}\text{Sps}_1$ ). Almandine increases from core to rim to  $\text{Alm}_{44}$ , pyrope increases to  $\text{Prp}_{36}$  at the inner rim and decreases to  $\text{Prp}_{31}$  at the outermost rim, and grossular decreases to  $\text{Grs}_{21}$  at the inner rim and increases to  $\text{Grs}_{22}$  at the outermost rim (Fig. 6a; Table 3). Spessartine is relatively constant at  $\text{Sps}_1$  and increases to  $\text{Sps}_2$  at the outermost rim. Grt II has similar composition to the rim of Grt I.

Clinopyroxene of variable composition is present as inclusions in garnet, in the matrix and in symplectite (Fig. 6b; Table 4). Inclusions in Grt I are omphacite, with  $X_{\text{Na}}$  [=  $\text{Na}/(\text{Na} + \text{Ca})$ ] up to 0.40. Matrix clinopyroxene varies from omphacite to diopside with a Na-rich core ( $X_{\text{Na}}$  up to 0.43–0.44) and a Na-poor rim ( $X_{\text{Na}} = 0.16$ ). Clinopyroxene in the symplectite is diopside.

All amphibole is calcic, specifically pargasite and sadanagaite (Fig. 6c; Table 5). Ferric iron, calculated using the charge balance method (Locock, 2014; Hawthorne et al., 2012), is < 0.40 p.f.u. (atoms per formula unit). Zoisite (Table 5) in garnet contains  $\text{Fe}^{3+}$  between 0.12 and 0.14 p.f.u., whereas matrix zoisite shows a slightly larger range, 0.10–0.14. No systematic zoning is seen in zoisite.

Feldspar includes both K-feldspar and plagioclase (Fig. 3; Tables 5, 6). The plagioclase inclusions in garnet are nearly

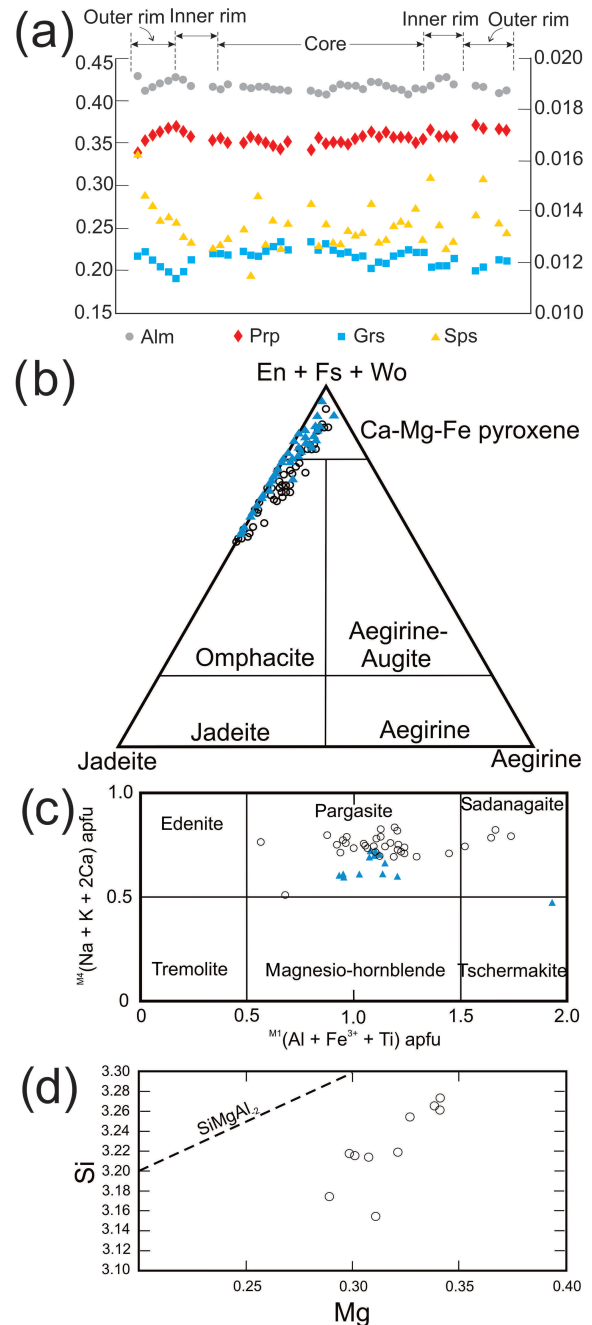


**Figure 6.** Diagrams showing compositional variation of garnet, clinopyroxene, amphibole and phengite. (a) Compositional zoning of garnet along the profile shown in Fig. 5a. Primary axis on the left is for Alm, Prp and Grs, whereas the secondary axis on the right is for Sps. (b) Ternary diagram showing composition of clinopyroxene varying from omphacite to diopside. Black circles are for analyzed mineral in 03-57, and blue triangles are for those in 03-59. (c)  $M^4(\text{Na} + \text{K} + 2\text{Ca})$  vs.  $M^1(\text{Al} + \text{Fe}^{3+} + \text{Ti})$  diagram showing amphibole chemistry, nomenclature follows Hawthorne et al. (2012); symbols are the same as (b). (d) Mg vs. Si p.f.u. diagram showing the composition of phengite in sample 03-57.

**Table 3.** Representative analyses of garnet from the samples 03-57 and 03-59. Vanadium was analyzed but its concentration is below the detection limit of the microprobe, and thus is neglected from the data. Garnet is normalized to 24 oxygen, with 10 six- and eight-fold coordinated cations. Ferric iron ( $\text{Fe}^{3+}$ ) is calculated based on a total of four atoms on the octahedrally coordinated site.

Comment Analysis	03-57			03-59		
	Core Gt1 no. 304	Inner rim Gt1 no. 286	Outer rim Gt1 no. 282	Core Gt1 no. 70	Inner rim Gt no. 49	Outer rim Gt1 no. 109
SiO <sub>2</sub>	39.33	38.90	39.07	39.14	39.50	39.40
TiO <sub>2</sub>	0.08	0.04	0.03	0.03	0.01	0.04
Al <sub>2</sub> O <sub>3</sub>	22.09	22.31	22.29	22.27	22.48	22.57
Cr <sub>2</sub> O <sub>3</sub>	0.03	0.00	0.12	0.00	0.03	0.01
FeO*	20.38	21.11	20.45	19.86	19.96	20.22
MnO	0.67	0.64	0.69	0.52	0.52	0.50
MgO	9.18	9.97	9.55	9.35	10.30	9.44
CaO	8.70	7.10	8.29	9.23	8.04	8.82
Na <sub>2</sub> O	0.00	0.01	0.04	0.00	0.00	0.01
Total	100.48	100.09	100.53	100.41	100.84	101.00
Si	5.90	5.81	5.81	5.83	5.84	5.84
Ti	0.01	0.00	0.00	0.00	0.00	0.00
Al	3.90	3.93	3.91	3.91	3.92	3.94
Cr	0.00	0.00	0.01	0.00	0.00	0.00
Fe <sup>3+</sup>	0.09	0.07	0.08	0.09	0.08	0.06
Fe <sup>2+</sup>	2.46	2.56	2.46	2.38	2.39	2.45
Mn	0.09	0.08	0.09	0.07	0.07	0.06
Mg	2.05	2.22	2.12	2.08	2.27	2.09
Ca	1.40	1.14	1.32	1.47	1.27	1.40
Na	0.00	0.00	0.01	0.00	0.00	0.00
Grossular	0.23	0.19	0.22	0.25	0.21	0.23
Pyrope	0.34	0.37	0.35	0.35	0.38	0.35
Almandine	0.41	0.43	0.41	0.40	0.40	0.41
Spessartine	0.01	0.01	0.01	0.01	0.01	0.01

All iron is treated as ferrous iron in the analytical results, as marked by the star (\*).

pure albite to oligoclase ( $X_{\text{An}}$ : 0.16–0.28). The matrix plagioclase is also oligoclase ( $X_{\text{An}}$ : 0.24–0.30). Plagioclase in symplectite is oligoclase and andesine ( $X_{\text{An}}$ : 0.28–0.33).

The pristine phengite inclusion in Grt I contains Si between 3.15 and 3.27 p.f.u. (Figs. 5e–f and 6d; Table 6). One analyzed phengite in a polyminerally inclusion in the rim of Grt I yielded a total of ~95.6 wt% and a Si content of 3.41 p.f.u. (Table 6). Kyanite contains a small amount of  $\text{Fe}^{3+}$ , up to 0.08 p.f.u. Rutile enclosed in garnet contains 470–840 ppm Zr, whereas the Zr content in matrix rutile ranges between 550 and 630 ppm.

#### 4.2.2 Zoisite eclogite 03-59

Garnet is slightly zoned, varying from  $\text{Prp}_{34}\text{Alm}_{41}\text{Grs}_{24}$  at the core to an inner rim of  $\text{Prp}_{38}\text{Alm}_{41}\text{Grs}_{22}$ ; the composition changes to  $\text{Prp}_{33}\text{Alm}_{41}\text{Grs}_{24}$  at the outermost rim. Spessartine is constant at ~1 mol%. Matrix clinopyroxene is omphacite ( $X_{\text{Na}}$  up to 0.43) in the core and diopside ( $X_{\text{Na}}$  =

0.14) in the rim (Table 4). Clinopyroxene in the symplectite is diopside (Fig. 6b).

Feldspar inclusions in clinopyroxene are oligoclase ( $X_{\text{An}} \approx 0.27$ ; Table 5). The matrix feldspar is also oligoclase ( $X_{\text{An}} = 0.24$ –0.30,  $X_{\text{kfs}} < 0.01$ ); the plagioclase displays a slight zoning with a lower anorthite core ( $X_{\text{An}} = 0.24$ ) and higher anorthite rim ( $X_{\text{An}} = 0.29$ ). Symplectitic plagioclase coexisting with biotite in pseudomorphs after phengite has  $X_{\text{An}} = 0.27$ . Plagioclase in symplectite after omphacite shows  $X_{\text{An}} = 0.28$ –0.31.

Amphibole is calcic, specifically pargasite and tschermakite (Fig. 6c; Table 5). Zoisite is slightly zoned with  $\text{Fe}^{3+}$  varying from 0.09 to 0.15 p.f.u. (all iron is assumed to be  $\text{Fe}^{3+}$ ). Kyanite inclusions in garnet contain up to 0.17 p.f.u.  $\text{Fe}^{3+}$ . Phengite in a polyminerally inclusion in garnet shows a total of ~94.7 wt% with a normalized composition with Si = 3.48 p.f.u. Matrix rutile contains 690 to 890 ppm Zr.

**Table 4.** Representative analyses of clinopyroxene in the zoisite eclogites 03-57 and 03-59. Ferric iron is calculated by charge balance, while Al<sub>T</sub> and Al<sub>O</sub> stand for aluminum in tetrahedral and octahedral sites, respectively. Clinopyroxene is normalized to six oxygen and four cations.

Comment	03-57			03-59		
	Core	Rim	Symplectite	Core	Rim	Symplectite
Analysis	gt4-12 no. 248	gt1-11 no. 47	no. 191	gt2-12 no. 26	gt2-12 no. 15	no. 15
SiO <sub>2</sub>	55.00	52.36	49.96	54.49	52.80	52.20
TiO <sub>2</sub>	0.17	0.14	0.39	0.12	0.27	0.33
Al <sub>2</sub> O <sub>3</sub>	11.88	7.47	8.03	12.49	7.85	5.85
Cr <sub>2</sub> O <sub>3</sub>	0.09	0.08	0.09	0.03	0.04	0.00
FeO	3.65	4.59	4.31	3.77	4.12	3.84
MnO	0.02	0.05	0.09	0.05	0.04	0.03
MgO	8.67	12.02	12.22	9.25	12.11	13.52
CaO	14.07	20.91	22.48	13.81	20.43	22.28
Na <sub>2</sub> O	6.20	2.43	1.50	5.76	2.46	1.51
K <sub>2</sub> O	0.01	0.00	0.00	0.18	0.01	0.01
Total	99.76	100.21	99.29	99.95	100.15	99.67
Si	1.96	1.90	1.84	1.94	1.91	1.91
Al <sub>T</sub>	0.04	0.10	0.16	0.06	0.09	0.09
Al <sub>O</sub>	0.46	0.22	0.19	0.46	0.25	0.16
Ti	0.00	0.00	0.01	0.00	0.01	0.01
Cr	0.00	0.00	0.00	0.00	0.00	0.00
Fe <sup>3+</sup>	0.00	0.04	0.06	0.00	0.00	0.03
Fe <sup>2+</sup>	0.11	0.10	0.07	0.11	0.12	0.09
Mn	0.00	0.00	0.00	0.00	0.00	0.00
Mg	0.46	0.65	0.67	0.49	0.65	0.74
Ca	0.54	0.81	0.89	0.53	0.79	0.87
Na	0.43	0.17	0.11	0.40	0.17	0.11
K	0.00	0.00	0.00	0.01	0.00	0.00
Na/(Na + Ca)	0.44	0.17	0.11	0.43	0.18	0.11

## 5 Isochemical phase equilibrium modeling

### 5.1 Modeling methods

Isochemical phase equilibrium modeling was conducted using the Gibbs free energy minimization method included in the software package PERPLE\_X ver. 6.7.7 (Connolly, 2005). Three  $P$ – $T$  phase diagrams were constructed for the sample 03-57 according to the following strategy. (i) The first pseudosection was modeled using the measured bulk rock composition with the 11-component system MnNCKFMASHTO (MnO–Na<sub>2</sub>O–CaO–K<sub>2</sub>O–FeO–MgO–Al<sub>2</sub>O<sub>3</sub>–SiO<sub>2</sub>–H<sub>2</sub>O–TiO<sub>2</sub>–O<sub>2</sub>). A small amount of oxygen, as a proxy for Fe<sub>2</sub>O<sub>3</sub> in the bulk rock, and a free fluid phase of pure H<sub>2</sub>O were added. This pseudosection was used to infer the initial melt composition to be added back to the measured bulk composition in order to obtain a melt-reintegrated bulk composition and to infer the retrograde evolution after the attainment of peak  $T$ . (ii) The second diagram was calculated in a reduced 8-component system MnNCFMASH to model a garnet-bearing melt-pocket (Fig. 3a). Mi-

crostructural evidence suggests that the studied samples were partially melted: the polymineralic inclusions in garnet and graphitic amphibole + plagioclase (Fig. 3b) and plagioclase + diopside + Grt II in the matrix (Fig. 3a) represent former melt pockets. Accordingly, this pseudosection was used to constrain peak  $T$ . (iii) An additional melt-reintegrated pseudosection was modeled with the MnNCKFMASHTO system to reconstruct the  $P$ – $T$  history before melt loss (i.e., before peak  $P$ ), by adding 10 % melt back to the measured bulk composition. The bulk composition changes if melt is lost from the system (Yakymchuk and Brown, 2014), particularly after reaching a threshold of 7 vol % (Rosenberg and Handy, 2005). Models can address this issue by integrating the estimated composition of lost melt back into the measured bulk composition (e.g., Bartoli, 2017, and references therein).

The internally consistent thermodynamic dataset of Holland and Powell (2011) for minerals and H<sub>2</sub>O (the CORK model; Holland and Powell, 1991) was used, together with solution models that are compatible with this dataset. The models include Omph(GHP) for Na-poor clinopyroxene and omphacite, cAmph(G) for clinoamphibole, melt (G) for melt

**Table 5.** Representative analyses of matrix minerals in the zoisite eclogite. The dash (–) refers to unanalyzed data, while b.d. refers to below detection limit. Ferric iron ( $\text{Fe}^{3+}$ ) in amphibole is calculated based on charge balance (see Locock, 2014, for details). All iron in feldspar and zoisite is assumed to be ferric.  $X\text{Fe}^{3+}$  is defined as  $100 * \text{Fe}^{3+} / (\text{Fe}^{3+} + \text{Al})$ . Feldspar is normalized to 8 oxygen, zoisite to 12.5 oxygen, and amphibole to 46 valences.

Mineral	03-57					03-59				
	Zo	Amp	Amp	Pl	Pl	Amp	Amp	Zo	Pl	
Comment	Matrix	Matrix	Matrix	Matrix	Symplectite	Matrix	Symplectite	Matrix	Matrix	
Analysis	M-13 no. 78	g3-12 no. 155	g4-11 no. 233	m no. 98	s310 no. 271	g4-cl no. 291	s21 no. 16	g3-12 no. 70	M-12pl	
$\text{SiO}_2$	39.44	37.83	43.82	60.73	60.03	43.21	45.63	39.06	59.52	
$\text{TiO}_2$	0.06	0.05	0.56	0.00	0.00	0.66	0.67	0.07	0.00	
$\text{Al}_2\text{O}_3$	32.08	21.61	14.66	24.44	25.62	15.03	12.05	32.17	24.91	
$\text{Cr}_2\text{O}_3$	0.05	0.07	0.09	0.01	0.00	0.06	0.00	0.03	0.00	
FeO	1.80	13.32	8.90	0.17	0.03	7.48	8.24	1.62	0.00	
MnO	0.00	0.25	0.04	b.d.	b.d.	0.03	0.04	0.03	b.d.	
MgO	0.04	9.49	14.53	0.05	0.01	14.62	14.87	0.08	0.01	
CaO	24.81	11.40	11.72	6.18	7.11	11.73	12.73	24.52	6.64	
$\text{Na}_2\text{O}$	0.00	2.75	2.47	8.42	7.79	2.44	1.72	0.02	7.93	
$\text{K}_2\text{O}$	–	0.61	0.91	0.05	0.05	0.84	0.48	–	0.17	
BaO	–	b.d.	b.d.	b.d.	b.d.	b.d.	0.02	–	b.d.	
Total	98.28	97.38	97.70	100.09	100.64	96.11	96.44	97.61	99.18	
Si	2.99	5.57	6.32	2.70	2.66	6.30	6.63	2.98	2.68	
Ti	0.00	0.01	0.60	0.00	0.00	0.07	0.07	0.00	0.00	
Al	2.87	3.75	2.49	1.28	1.34	2.58	2.06	2.90	1.32	
Cr	0.00	0.00	0.01	0.00	0.00	0.01	0.00	0.00	0.00	
$\text{Fe}^{3+}$	0.11	0.40	0.13	0.01	0.00	0.08	0.00	0.10	0.00	
$\text{Fe}^{2+}$	–	1.18	0.88	0.00	0.00	0.83	1.00	–	0.00	
Mn	0.00	0.03	0.01	b.d.	b.d.	0.00	0.01	0.00	b.d.	
Mg	0.00	2.09	3.12	0.00	0.00	3.18	3.22	0.01	0.00	
Ca	2.02	1.80	1.81	0.29	0.34	1.83	1.98	2.01	0.32	
Na	0.00	0.79	0.69	0.73	0.67	0.69	0.49	0.00	0.69	
K	–	0.12	0.17	0.00	0.00	0.16	0.09	–	0.01	
Ba	–	b.d.	b.d.	b.d.	b.d.	b.d.	0.00	–	b.d.	
$X\text{Fe}^{3+}$	3.69							3.45		
$\text{Na}/(\text{Na} + \text{Ca})$				0.71	0.66				0.68	

(Green et al., 2016), Gt(W) for garnet, Mica(W) for potassic white mica (e.g., phengite) and paragonite, Bi(W) for biotite, Chl(W) for chlorite (White et al., 2014), T for talc (Holland and Powell, 2011), and feldspar for both plagioclase and K-feldspar (Fuhrman and Lindsley, 1988). Garnet contains a small amount of spessartine, and thus this end-member was restricted to 10 mol% in the solution model. Lawsonite, quartz, zoisite and kyanite were treated as pure phases. The applied melt model was originally developed for  $P < 1.3$  GPa but has been extrapolated to 2.6 GPa with geologically meaningful results (Wade et al., 2017). The compositional ranges of the amphibole and melt models were limited iteratively during the calculations. The keyword values for initial\_resolution, final\_resolution, iteration value 2 and refinement\_points\_II in the perplex\_option.data file were set at 0.100, 5e-3, 1 and 1, respectively, minimizing the number of pseudocompounds during calculation.

## 5.2 Modeling results

### 5.2.1 Pseudosection for the measured bulk rock composition

The composition of the bulk rock for sample 03-57 was acquired using wavelength-dispersive X-ray fluorescence (XRF) spectrometry at Washington State University. The analyzed bulk composition was adjusted for PERPLE\_X in the chosen systems (Table 7). CaO was reduced by the amount of corresponding  $\text{P}_2\text{O}_5$ , assuming that all phosphorus is bound to ideal apatite. The initial water used is 0.75 wt %, estimated using the water content (Schmidt and Poli, 2014), density and proportion of hydrous minerals. Since a small amount of ferric iron is present in omphacite, kyanite, zoisite and amphibole, the oxygen content was estimated corresponding to 10 % of total iron being trivalent. The total components were normalized to 100 %.

The  $P$ – $T$  pseudosection was calculated for the range of 1.0–2.5 GPa and 600–950 °C (Fig. 7 and Fig. S1 in the Supplement). Garnet and clinopyroxene are ubiquitous in the modeled phase diagram. The solidus curve shows a posi-

**Table 6.** Representative analyses of minerals in garnet in the zoisite eclogite 03-57. Ph<sup>1</sup> is the pristine phengite (Fig. 6) and Ph<sup>2</sup> occurs as a mineral in polymineralic inclusion in garnet. The dash (–) marks unanalyzed elements, while b.d. marks those below detection limit. Structural formulae for minerals other than phengite were calculated as given in Tables 4 and 5. Phengite is recalculated based on 42 valences for the four- and six-fold cations.

Mineral Analysis	Omp no. 99	Ph <sup>1</sup> Ph no. 10	Ph <sup>2</sup> g3-138 no. 111	Kfs g1-i no. 2	Pl g1-i no. 21	Amp g3i no. 47	Zo g4i no. 219
SiO <sub>2</sub>	54.14	49.56	52.09	64.24	65.08	49.23	38.81
TiO <sub>2</sub>	0.12	0.98	0.14	0.00	0.01	0.03	0.06
Al <sub>2</sub> O <sub>3</sub>	11.88	29.48	28.01	18.31	21.05	35.01	32.27
Cr <sub>2</sub> O <sub>3</sub>	0.00	0.00	0.01	0.00	0.01	0.03	0.00
FeO	3.85	1.27	1.78	0.30	1.30	1.67	1.92
MnO	0.07	0.01	b.d.	b.d.	0.10	0.05	b.d.
MgO	9.00	3.46	3.39	0.02	0.10	1.56	0.05
CaO	15.03	0.02	0.05	0.08	3.49	1.57	24.46
Na <sub>2</sub> O	5.63	0.39	0.01	0.10	10.19	1.76	0.03
K <sub>2</sub> O	0.10	10.56	10.10	17.03	0.06	5.35	–
BaO	–	0.39	b.d.	b.d.	b.d.	b.d.	–
Total	99.82	96.11	95.58	100.10	101.54	96.27	97.60
Si	1.93	6.55	6.82	2.98	2.85	6.62	2.97
Ti	0.00	0.10	0.01	0.00	0.00	0.00	0.00
Al	0.50	4.59	4.32	1.00	1.08	5.55	2.91
Cr	0.00	0.00	0.00	0.00	0.00	0.00	0.00
Fe <sup>3+</sup>	0.02	0.00	0.00	0.01	0.05	0.00	0.12
Fe <sup>2+</sup>	0.09	0.14	0.19	–	–	0.19	–
Mn	0.00	0.00	0.00	0.00	0.00	0.01	0.00
Mg	0.48	0.68	0.66	0.00	0.00	0.31	0.01
Ca	0.57	0.00	0.01	0.00	0.16	0.23	2.00
Na	0.39	0.10	0.00	0.01	0.86	0.46	0.00
K	0.00	1.78	1.69	1.01	0.00	0.92	–
Ba	–	0.02	0.00	0.00	0.00	0.00	–
Na/(Na + Ca)	0.40			0.69	0.84		

**Table 7.** Whole rock bulk composition determined by X-ray fluorescence (XRF), along with adjusted bulk composition; domainal composition of a melt pocket; reintegrated melt composition at 2.2 GPa, 802 °C; and melt-reintegrated composition for sample 03-57 that are used for modeling. All are given in weight percentages (wt %). The amount of O<sub>2</sub> for the adjusted bulk rock is estimated to be equivalent to 10 % Fe<sup>3+</sup> of total iron. The dash (–) marks the elements not determined or considered.

	XRF data	Adjusted bulk rock	Melt pocket	Reintegrated melt	Melt-reintegrated
SiO <sub>2</sub>	50.62	50.324	50.265	59.444	51.217
TiO <sub>2</sub>	0.226	0.225	–	–	0.203
Al <sub>2</sub> O <sub>3</sub>	19.72	19.605	21.868	14.789	19.140
FeO*	5.60	5.569	9.044	0.062	5.018
MnO	0.113	0.112	0.289	–	0.101
MgO	7.66	7.618	5.007	0.028	6.859
CaO	11.74	11.567	8.088	1.514	10.561
Na <sub>2</sub> O	3.83	3.810	4.438	4.852	3.995
K <sub>2</sub> O	0.36	0.360	–	2.289	0.478
P <sub>2</sub> O <sub>5</sub>	0.084	–	–	–	–
O <sub>2</sub>	–	0.062	–	–	0.056
H <sub>2</sub> O	–	0.750	1.000	17.022	2.374
Sum	99.96	100.00	100.00	100.00	100.00
LOI (%)	0.36	–	–	–	–

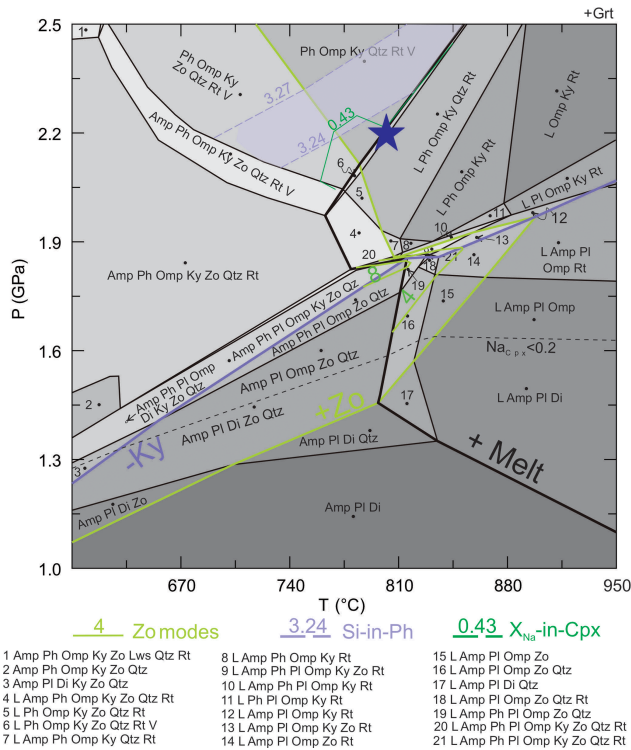


**Figure 7.**  $P$ – $T$  pseudosection of sample 03-57 with an XRF-derived bulk composition, showing the mineral assemblages and highlighted phase boundaries of kyanite, zoisite, melt (L). Abbreviations are in Table 1; V = free water. Dashed line of  $Na_{Cpx}$  indicates Na content in M2 site in clinopyroxene; the line separates the mineral assemblages with calcic pyroxene (augite,  $Na_{Cpx} < 0.20$ ) from those with sodic–calcic pyroxene (omphacite,  $Na_{Cpx} > 0.20$ ). The purple area marks where the highest values of Si-in-Ph and  $X_{Na}$ -in-Cpx intersect. This area provides an estimate of peak  $P$  to use in determining a  $P$ – $T$  path across which an initial melt that is reintegrated into bulk composition is generated (marked by the blue star). Zoisite modes at 1.7–1.9 GPa, 800–880 °C are also marked.

tive  $dP/dT$  slope at  $P > 1.95$  GPa and a negative slope at  $P < 1.4$  GPa (Fig. 7). Melt is only present at  $T > 750$  °C; the highest amount of melt predicted within the  $P$ – $T$  range is 12 % at 2.0 GPa, 900 °C. This pseudosection cannot be used to retrieve  $P$ – $T$  conditions before melt loss.

To estimate the approximate prograde path prior to melt loss, a certain amount of melt needs to be reintegrated into the measured bulk composition. The melt reintegrated pseudosection is used to estimate a prograde path across which an initial melt was generated. In this case, the estimated peak conditions are not the true peak and are used solely for deriving a  $P$ – $T$  path that crosses the solidus, where initial melt composition (Table 7) is determined for modeling a melt reintegrated pseudosection. Using isopleths of Si-in-phengite and  $X_{Na}$ -in-clinopyroxene, the phengite with average high Si content (3.24–3.27 p.f.u.) and the omphacite with average high  $X_{Na}$  value (0.43–0.44) intersect at  $2.3 \pm 0.2$  GPa,

$770 \pm 60$  °C. The composition of the initial melt to be reintegrated into the measured bulk composition was granitic sensu lato and determined at  $P = 2.2$  GPa and  $T = 800$  °C.

The pseudosection modeled with the measured bulk rock composition yields additional  $P$ – $T$  conditions, based on the observed zoisite-bearing textures. Zoisite overgrowths on kyanite (e.g., Fig. 3b, c) indicate that the rock followed a path that leads to increasing modes of zoisite and decreasing modes of kyanite. The pseudosection predicts that, at 800–900 °C, the kyanite-out and the zoisite-in boundaries are nearly parallel and located close to each other, thus defining narrow fields containing both phases at 1.9–2.1 GPa. These Ky + Zo-bearing fields represent a nearly discontinuous reaction that consumes kyanite and produces zoisite at decreasing pressure. The observed kyanite–zoisite relationship suggests that the rock followed a  $P$ – $T$  path that crossed this reaction. Moreover, the anhedral shape of zoisite adjacent to leucocratic layers of crystallized melt suggests that the sample traversed through areas of zoisite-melting located at  $P = 1.7$ –2.0 GPa and  $T = 800$ –900 °C (Fig. 7).

### 5.2.2 Pseudosection for a crystallized melt pocket

A crystallized melt pocket (Fig. 3a) was modeled to determine the equilibrium conditions for melting (i.e., peak- $T$  conditions). Bulk composition (Table 7) for the crystallized melt pocket (Figs. 3a, 8) was calculated with estimated modes of 35 % peritectic garnet, 55 % plagioclase and 10 % clinopyroxene along with their corresponding mineral composition. Phase densities used are  $2.64 \text{ g cm}^{-3}$  for plagioclase (Phillips et al., 1971),  $3.29 \text{ g cm}^{-3}$  for clinopyroxene (Mottana et al., 1979) and  $3.7 \text{ g cm}^{-3}$  for garnet (Nestola et al., 2012) because the experimental mineral composition is similar to those in the crystallized melt pocket. An arbitrary value of 1 wt % water was used. The pseudosection calculated with this estimated bulk composition shows that the assemblage of garnet, plagioclase, omphacite and melt is located at 1.9–2.2 GPa and 850–950 °C within the modeled  $P$ – $T$  range (Figs. 8, S2). The isopleths of  $X_{Mg}$ -in-garnet,  $X_{Fe}$ -in-garnet and  $X_{Na}$ -in-plagioclase do not intersect at a point, but in an area of  $1.9 \pm 0.2$  GPa,  $900 \pm 50$  °C, which is interpreted as the approximate peak  $T$  condition.

### 5.2.3 Pseudosection for melt-reintegrated composition

The petrographic textures (e.g., thin leucocratic layers interpreted as melt channels) in sample 03-57 suggest a small amount of melt loss. An accurate estimate of melt loss is difficult to determine (e.g., Indares et al., 2008), but a value of 10 % is used, based on the proportion of leucocratic layers in the sample. The melt-reintegrated pseudosection returns the solidus to water-saturated conditions (Groppo et al., 2012; Indares et al., 2008). The bulk composition (Table 7) used to calculate this pseudosection (Figs. 9, S3) reintegrated 10 vol % of melt into the measured bulk rock using a single-

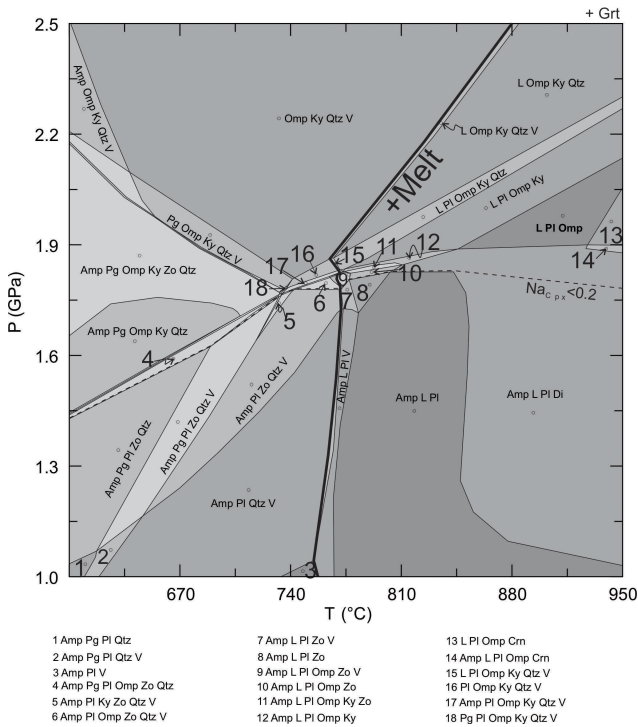


**Figure 8.** *P*–*T* pseudosection modeled for a melt domain in zoisite eclogite 03-57; the solidus curve is highlighted. The field with the observed mineral assemblage of garnet, plagioclase, omphacite and melt are shown with bold fonts at 1.9–2.1 GPa, 850–950 °C. The dashed line of NaC<sub>px</sub> and abbreviations are the same as in Fig. 7.

step approach (e.g., Indares et al., 2008; Bartoli, 2017). The melt composition (Table 7) that was added back into the measured bulk rock is derived from the first pseudosection at the potential peak *P* (see Sect. 5.2.1). This represents the first melt produced by the source. Since the suprasolidus topology does not significantly change in response to bulk composition due to melt loss (White and Powell, 2002), reintegration of the escaped melt with the residual rock would approach the original rock composition.

The melt-reintegrated pseudosection shows that the observed peak mineral assemblage of garnet, omphacite, phengite, kyanite, quartz and rutile is predicted to be stable at 2.1–2.5 GPa, 720–850 °C (Fig. 9), which is located in a similar *P*–*T* range as predicted by the pseudosection modeled with the measured bulk rock composition (Table 7; Fig. 7). Isopleths of phengite included in garnet (Si = 3.24–3.27) and omphacite (*X*<sub>Na</sub> = 0.43–0.44) yielded a peak *P* of 2.4 ± 0.1 GPa at 830 ± 30 °C (Fig. 9). Additionally, paragonite is predicted to have been present at *P* = 1.3–2.0 GPa and *T* = 600–730 °C. To form the melting textures with Na- and K-rich phases (e.g., albite and K-feldspar) in garnet, Na- and K-rich sources are needed; paragonite and phengite predicted by the pseudosection are the best candidates. Therefore, the

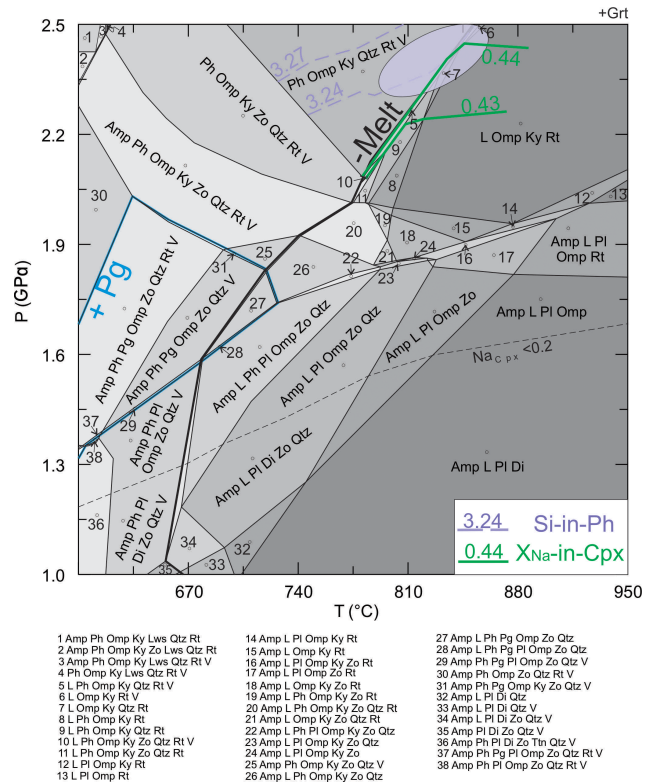


**Figure 9.** Calculated *P*–*T* phase diagram modeled with a melt-reintegrated composition of sample 03-57. The pseudosection is highlighted for the phase boundaries of paragonite (Pg) and melt, and is saturated with fluid at subsolidus conditions. Isoleths of Si-in-Ph and *X*<sub>Na</sub>-in-Cpx are plotted on the modeled diagram, with the ellipse indicating where determined compositions intersect at peak *P*. The dashed line of NaC<sub>px</sub> and mineral abbreviations are the same as in Fig. 7.

prograde path of the zoisite eclogite is interpreted to have passed through the paragonite- and phengite-present fields.

Integrating results from the three pseudosections, eclogite 03-57 displays a clockwise *P*–*T* path (Fig. 10). On the prograde path, paragonite formed in the *P*–*T* range of 1.3–2.0 GPa, 600–730 °C and phengite was present in the sample, while garnet grew and included both minerals (Fig. 9). The sample reached peak *P* of 2.4 ± 0.1 GPa at 830 ± 30 °C. The mineral assemblage of garnet + omphacite + kyanite + zoisite + phengite + quartz + rutile ± melt formed at these *P*–*T* conditions (Fig. 7). With subsequent exhumation and increase in *T*, partial melting occurred both in the matrix and in garnet (Figs. 3, 4) resulting in the formation of new peritectic garnet (Fig. 3a). The pseudosection modeled for a crystallized melt pocket suggests that a peak *T* of 900 ± 50 °C was attained at 1.9 ± 0.2 GPa (Fig. 8).

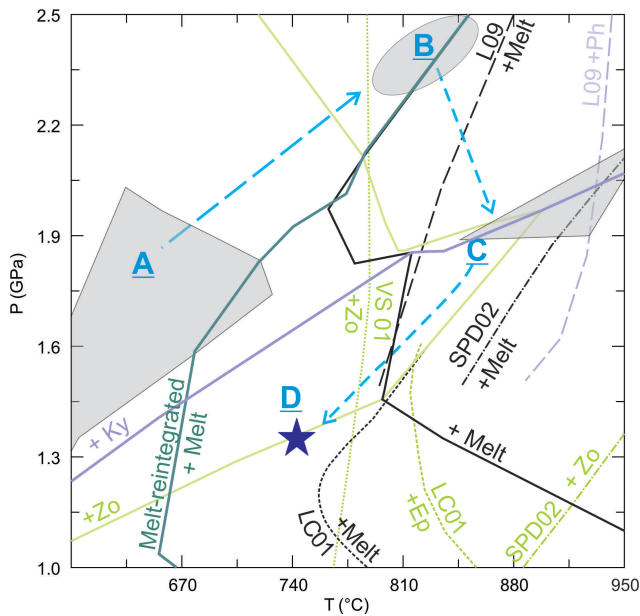


**Figure 10.**  $P$ – $T$  phase diagram showing the delineated  $P$ – $T$  path (dashed light blue curves) for the studied eclogites along with modeled and experimental phase relations. A to D mark the determined  $P$ – $T$  stages, with the polygons, ellipse and star referring to determined  $P$ – $T$  conditions. A marks the  $P$ – $T$  field where paragonite is present. B is determined by the intersection of Si-in-phengite and  $X_{\text{Na}}$ -in-Cpx. C refers to the  $P$ – $T$  conditions where zoisite grew at the expense of kyanite and the stable assemblage of the modeled melt pocket. The star at D is determined using empirical amphibole-plagioclase thermometry and Al-in-hornblende barometry. Phase boundaries of solidus (black), kyanite and zoisite from pseudosection of measured bulk composition, and solidus (dark green) from melt-reintegrated pseudosection are shown by solid lines. The theoretical phase boundary of zoisite by Vielzeuf and Schmidt (2001) (VS01) is the dotted line. Long dashed lines marked as L09 represent phase boundaries of melt and phengite in experiments by Liu et al. (2009) on phengite-zoisite eclogite, whereas dot-dashed lines (SPD02) are from Skjærli and Patiño Douce (2002) on zoisite eclogites, and short dashed lines (LC01) are from Lopez and Castro (2001) on amphibolite.

## 6 Empirical thermobarometry and trace element thermometry

### 6.1 Empirical thermobarometry

Empirical garnet-clinopyroxene-phengite-kyanite-SiO<sub>2</sub> thermobarometry (Ravna and Terry, 2004) was used to estimate equilibrium conditions for sample 03-57. Omphacite with the highest jadeite content ( $X_{\text{Na}} = 0.43$ – $0.44$ ), pristine phengite (Si p.f.u.: 3.24–3.27) and garnet with the highest  $X_{\text{Prp}}$  value (Alm<sub>43</sub>Prp<sub>37</sub>Grs<sub>19</sub>) return an equilibrium  $P$ – $T$  condition of 2.57 GPa, 818 °C. Uncertainties in the original garnet-phengite-clinopyroxene-kyanite-quartz thermobarometry are  $\pm 0.32$  GPa and  $\pm 65$  °C (Ravna and Terry, 2004). Pressure calculated by empirical thermobarometry is within the range

of error of the  $P$ – $T$  results from the pseudosection ( $2.4 \pm 0.1$  GPa,  $830 \pm 30$  °C).

Hornblende-plagioclase thermometry by Holland and Blundy (1994) and Al-in-hornblende barometry (Anderson and Smith, 1995) are used iteratively to retrieve exhumation conditions. The crystallized melt pocket does not contain quartz, hence we used the calibration based on the net-transfer reaction edenite + albite = richterite + anorthite. Uncertainty for the amphibole-plagioclase thermometry is given as  $\pm 40$  °C with potential larger errors for Fe-rich amphibole (Holland and Blundy, 1994), and for the Al-in-hornblende barometry it is 0.06 GPa (Anderson and Smith, 1995). The calculation with oligoclase ( $X_{\text{Ab}} = 0.71$ ) and sadanagaitic amphibole (Table 5) yielded crystallization at  $\sim 1.3$  GPa, 750 °C.

### 6.2 Zr-in-rutile thermometry

Zirconium incorporation in rutile, in equilibrium with quartz and zircon, has been developed into an empirical single mineral thermometer (Zack et al., 2004) and experimentally calibrated to incorporate the pressure effect (Tomkins et al., 2007; Watson et al., 2006). The studied eclogites contain zircon and quartz, which renders the thermometry suitable to obtain crystallization temperatures. Conditions determined by pseudosections fall within the  $\alpha$ -quartz field, thus the Zr-in-rutile thermometry for this field is used (Tomkins et al., 2007). At peak  $P$  of 2.4 GPa, rutile inclusions in garnet in sample 03-57 yielded a  $T$  range of 723–777 °C, while matrix rutile gave  $T = 737$ – $749$  °C (Tomkins et al., 2007). At  $P = 1.3$  GPa, the thermometer returns a  $T$  at 674–726 °C for rutile inclusions and 688–700 °C for matrix rutile. For sample 03-59, the thermometer gives  $T$  ranges of 684–784 °C at peak  $P$  of 2.4 GPa and 639–734 °C at 1.3 GPa. Uncertainty of the thermometry has been estimated to be  $\sim 30$  °C (Tomkins et al., 2007).

## 7 Discussion

### 7.1 Prograde to peak $P$ stages

Retrieving the exact prograde  $P$ – $T$  path for the studied samples is difficult because much of the prograde information has been lost during melting at high  $T$ ; however,  $P$ – $T$  pseudosections modeled with melt-reintegrated compositions could yield critical information on the prograde path (e.g., Indares et al., 2008). Although one-step or multi-step approaches have been proposed to reintegrate melt compositions, they yield similar overall topologies of the modeled phase diagrams (Bartoli, 2017). By a one-step melt-reintegration approach, the modeled pseudosection (Fig. 9) shows that a few restricted fields with paragonite occur on the prograde path. Abundant crystallized melt pockets with albite found in garnet, interpreted as being formed through melting of paragonite inclusions (see Sect. 7.2.1 for detailed discus-

sion), require the former presence of paragonite during garnet growth. Thus, the prograde  $P$ – $T$  path is interpreted to traverse paragonite-present  $P$ – $T$  fields at 1.3–2.1 GPa, 600–740 °C (field A in Fig. 10).

Previous studies suggested a broad range for peak  $P$  of the NEGEP: 1.8–2.3 GPa for garnet websterite from the central block (Brueckner et al., 1998) and 1.6–2.0 GPa for kyanite eclogite from Weinschenk Island (~20 km to the south of Sanddal) in the central block (Elvevold and Gilotti, 2000). This study used forward isochemical phase equilibrium modeling along with mineral isopleths to generate reliable  $P$ – $T$  conditions based on mineral composition (Massonne, 2013; Powell and Holland, 2008). The melt-reintegrated pseudosection, along with pristine phengite with average high Si (3.24–3.27 p.f.u.) and omphacite with average high  $X_{\text{Na}}$  (0.43–0.44), yielded peak  $P$  of  $2.4 \pm 0.1$  GPa at  $830 \pm 30$  °C (Fig. 9). This estimated  $P$ – $T$  range is located across the solidus; therefore, it is likely that a small fraction of melt (< 7 vol %) was already present at peak  $P$ . The  $P$ – $T$  estimates are well within the range of error for garnet-clinopyroxene-kyanite-phengite-quartz thermobarometry ( $2.57 \pm 0.32$  GPa,  $818 \pm 65$  °C).

The prograde to peak  $P$  path is also supported by temperature estimated from Zr-in-rutile thermometry. The rutile in both garnet and in the matrix is interpreted to have formed from prograde to potentially maximum  $T$  at higher  $P$ , because pseudosections using both the measured and melt-reintegrated bulk composition do not show the presence of rutile at lower  $P$  conditions (Figs. 7, 9). The rutile in garnet yielded temperatures of 674–726 °C at 1.3 GPa and 723–777 °C at 2.4 GPa, which are within the prograde conditions estimated on the basis of the paragonite-present fields. Matrix rutile yields a  $T$  range at 737–749 °C in sample 03-57 and 684–784 °C in sample 03-59 at 2.4 GPa (i.e., at peak  $P$ ). This  $T$  range is slightly lower than the estimates from pseudosections, similar to previous research using this thermometry (e.g., Tual et al., 2018; Liu et al., 2015); this discrepancy can be attributed to diffusion modification of Zr concentration, kinetic effects in chemical disequilibrium, inaccuracy in the thermometry calibration or the application of pseudosection modeling or a combination of these processes (e.g., Tual et al., 2018; Liu et al., 2015).

## 7.2 Exhumation and partial melting stages

### 7.2.1 Evidence of partial melting

Concordant and discordant leucocratic veins within the eclogite pod and foliated eclogite in the margin are mesoscopic evidence that partial melting occurred in these rocks. The thickness of the leucosomes varies from millimeter to centimeter scales; the leucosomes merge from thinner into thicker veins (Fig. 2), which indicate that they originated internally. Potential melt channels (e.g., Fig. 3b) suggest that modes could have reached the threshold (7 %; Rosenberg and

Handy, 2005) for melt loss. Zoisite eclogite 03-59 from the margin of the pod has a strong L-S fabric defined by quartzofeldspathic layers and elongate zoisite grains (Figs. 2, 3) that possibly represents melt migration channels, with the original composition altered by melt loss to (or melt gain from) adjacent parts.

At the microscopic scale, areas marked by interstitial plagioclase, peritectic minerals and graphic intergrowth are interpreted as former melt pockets. Interstitial plagioclase in the crystallized melt pockets shows low dihedral angles (< 60°) at plagioclase solid–solid boundaries and is interpreted as original melt–solid boundaries, where plagioclase formed by crystallization of melt at surrounding solids such as garnet, zoisite or clinopyroxene (Holness and Sawyer, 2008). Such cusped boundaries are present in all studied samples (Fig. 3), regardless of the degree of melting. Small euhedral garnet (e.g., in 03-59) adjacent to plagioclase with typical cusped contacts and subhedral garnet with euhedral crystal faces in 03-57 are interpreted to have formed and/or grown as a peritectic phase during partial melting. Graphic amphibole and plagioclase intergrowths crystallized from a hydrous melt because undercooling can lead to epitaxial growth of minerals along earlier formed grains (e.g., Fenn, 1986; London and Morgan, 2012). The quartzofeldspathic layers in sample 03-59 contain abundant euhedral garnet crystals and cusped boundaries with plagioclase that formed during partial melting and subsequent cooling.

Polymineralic inclusions in garnet in HP and UHP eclogites have been interpreted to form via various mechanisms, for example, partial melting after entrapment of inclusion (Perchuk et al., 2005, 2008; Cao et al., 2019), trapped and crystallized melt (Ferrero et al., 2015; Chen et al., 2014; Ferrando et al., 2005; Stöckhert et al., 2001, 2009; Liu et al., 2013), and reaction between infiltrating fluids and precursor minerals (Liu et al., 2018). The polymineralic inclusions do not contain complex inclusion assemblages from fluid leaching of the host mineral and thus are not products of fluid interaction but melt crystallization. These inclusions are present throughout Grt I; if polymineralic inclusions represent trapped and crystallized melt, the inclusion process would require significant garnet growth (> 20 vol %) at melt-present conditions, which is not the case for the studied eclogites (5 vol %–7 vol % increase, according to the modeling results; see Fig. S1c). Therefore, the polymineralic inclusions are interpreted as crystallized melt generated from in situ melting of preexisting minerals in garnet. The polymineralic inclusions typically contain albite, K-feldspar, kyanite, phengite and quartz (Fig. 4), which requires the preexisting minerals to contain significant Na and K. A single phase of a nominally anhydrous mineral such as plagioclase, omphacite or K-feldspar is unlikely to melt at the peak conditions; the hydrous minerals paragonite and phengite are strong candidates to form Na- and K-rich melt. Melting of the inclusions led to volume expansion, which cracked the host mineral (Fig. 4). Melt migrated along intragranular frac-

tures into the matrix, leaving restitic minerals in the cracks (Fig. 3d). Droplets of melt migrated into the matrix adjacent to large garnet and crystallized, forming sharp offshoots into host minerals (Fig. 3d). New garnet was generated by melting and modified by high- $T$  diffusion, forming the observed patchy zoning (Fig. 5; Perchuk et al., 2008).

### 7.2.2 Melting reactions

The exact melting reactions cannot be determined from the polymineralic inclusions in garnet (Fig. 4) due to the lack of original reactant phases. Documented mineral phases and the  $P$ – $T$  history predicted by the pseudosections are needed. Crystallized melt pockets in the matrix commonly contain reactants and products, and thus can be used to interpret melting reactions using pseudosections.

Melting via paragonite and phengite breakdown occurred in garnet. Both minerals are predicted on the prograde path by the melt-reintegrated pseudosection (Fig. 9) and can be captured along with other minerals during garnet growth and preserved in the robust host mineral at higher  $P$ . Melting of paragonite and phengite with additional minerals occurred in garnet after reaching their breakdown temperatures and generated melt, kyanite and other minerals, for instance, by the following reactions: white mica + quartz  $\rightarrow$  K-feldspar + kyanite + melt (Lang and Gilotti, 2007; Huang and Wyllie, 1974) and phengite + clinopyroxene + quartz  $\rightarrow$  garnet + kyanite + melt (Hermann and Green, 2001).

In contrast, phengite and zoisite breakdown melting occurred in the matrix. A few crystallized melt pockets (e.g., Fig. 3d) with a granitic composition and sharp offshoots are interpreted as crystallized melt derived from phengite breakdown. The mineral assemblage Grt II + Ky + Kfs + Ab can form via the following reaction: phengite + clinopyroxene + quartz  $\rightarrow$  garnet + kyanite + melt (Hermann and Green, 2001), where the melt crystallizes to albite and K-feldspar in pockets. The abundant crystallized pockets of melt consisting of amphibole and plagioclase that are present between anhedral zoisite and diopside (Fig. 3b, c) suggest that the eclogites were partially melted through the following reaction: zoisite + omphacite + quartz  $\rightarrow$  melt + Na-poor clinopyroxene + garnet. Zoisite and omphacite were the remaining reactants during the partial melting, whereas diopside, euhedral garnet and melt were products. The melt later crystallized as oligoclase ( $X_{An} = 0.29$ ) and pargasitic amphibole. This zoisite melting reaction is similar to those suggested by Skjerlie and Patiño Douce (2002).

### 7.2.3 Partial melting conditions

The zoisite eclogites have undergone multi-stage partial melting, as suggested by textures and pseudosections. One stage of partial melting may have occurred only in garnet after paragonite entrapment at  $P$ – $T$  conditions outside of paragonite-present fields (Fig. 10); however, the exact

$P$ – $T$  could not be determined. The inclusions could have been shielded by the strong host mineral, avoiding pressure-induced breakdown, but then melted in response to increasing temperature. Phengite in both garnet and the matrix may have melted to form peritectic garnet, which then captured residual phengite grains. The initial melting may have occurred at peak  $P = 2.4$  GPa via phengite breakdown, according to the melt-reintegrated pseudosection (B in Fig. 10).

Another important stage of partial melting involves zoisite breakdown. Zoisite is predicted to be absent at peak  $P$  using the melt-reintegrated pseudosection (Fig. 9) but is present in the studied rocks, indicating its formation on the exhumation path (Fig. 7). Zoisite typically forms a corona around kyanite, suggesting consumption of the aluminosilicate and Ca from other minerals or the melt. Such reactions would be reflected as decreasing modal kyanite and increasing modal zoisite, which is predicted at 1.9–2.1 GPa, 800–900 °C. With continued exhumation, zoisite melts along with additional phases (e.g., omphacite), generating calcic melt at  $P < 1.9$  GPa (Figs. S1 and 10c).

The availability of fluid in the shear zone may have been critical in determining different degrees of partial melting in different parts of the outcrop. The zoisite eclogite 03-57, collected from the inner part of the eclogite pod, experienced a lower degree of partial melting, as evidenced by the smaller number of crystallized melt pockets. With limited availability of free fluid, the core of the eclogite pod partially melted through the in situ and localized breakdown of hydrous phases. In contrast, sample 03-59 from the margin of the pod shows a strong fabric, which might be due to combined fluid-absent and fluid-present melting. The outer eclogite pod might have suffered fluid-absent hydrous mineral-breakdown melting, evidenced by peritectic garnet, forming leucocratic layers. Fluid may have also infiltrated the eclogite pod, triggering partial melting and forming high modal zoisite, essentially generating a higher degree of partial melting than the center of the pod.

### 7.3 Cooling stage

Cooling of the HP terrane led to crystallization of melt pockets both in garnet and matrix. At peak  $T$  ( $\sim 900$  °C), the garnet rim equilibrated with the bulk rock. At least  $> 7$  vol % of melt was also formed (Fig. 7), perhaps leading to extraction along melt channels. That the melt pockets crystallized at pressures below the jadeite + quartz = albite reaction is indicated by the presence of plagioclase (Fig. 3). The cooling rate from peak  $T$  was probably low, and the presence of graphic intergrowths points to undercooling, typical for epitaxial growth of minerals (London and Morgan, 2012). Empirical hornblende-plagioclase thermometry yielded a temperature of  $\sim 750$  °C, which is close to the solidus on the modeled pseudosection (Fig. 7). Vermicular symplectite of diopside, plagioclase and amphibole replaced omphacite during this stage.

#### 7.4 Implications for eclogite melting

Hydrous minerals are critical to partial melting of metabasite at elevated pressure due to the absence of free water in orogenic lower crust. This process is commonly termed dehydration melting because the breakdown of OH-bearing minerals releases free water into the system, triggering partial melting of the host rock. Phengite is regarded as an important K-bearing phase that leads to partial melting of metabasite at HP and UHP, as demonstrated by experimental studies (Liu et al., 2009; Skjerlie and Patiño Douce, 2002) and in natural metabasites (Wang et al., 2014; Deng et al., 2019). Paragonite, common in medium-temperature HP eclogites (Massonne and Sobiech, 2007), is absent in the studied eclogite but is predicted on the melt-reintegrated pseudosection (Fig. 9) and documented in eclogite from nearby Weinschenk Island (Fig. 1; Elvevold and Gilotti, 2000). This Na-rich mica accounts for the albite-bearing polymineralic inclusions and Na-rich melt in the studied samples and has been argued to be a major contributor to partial melting of UHP eclogite from the Sulu belt, eastern China (Chen et al., 2014). Similarly, epidote-group minerals can break down and induce partial melting of calcic eclogite. The contribution of this melting depends on bulk composition. Melting by zoisite breakdown in the Sulu UHP eclogites was insignificant (Chen et al., 2014), but an epidote-group mineral is critical to melting UHP kyanite eclogite (Cao et al., 2019) and the studied zoisite eclogites. The remarkably preserved crystallized melt pockets in the studied samples indicate that zoisite was a significant contributor to anatexis. Zoisite with domains of growth and resorption in HP pegmatite from the Variscan Münchberg Massif (Germany) was interpreted to have formed through heating on the exhumation path (Liebscher et al., 2007).

Thermodynamic models of minerals and tonalitic melt (Green et al., 2016) provided a critical framework and extended the modeling capabilities to melting of metabasites (Hernández-Urbe et al., 2020; Palin et al., 2016a, b); however, problems still exist. Phase relations of phengite, zoisite and melt in the modeled pseudosection (Fig. 10) show discrepancies with the theoretically calculated (Vielzeuf and Schmidt, 2001) and experimentally determined  $P$ – $T$  boundaries (Lopez and Castro, 2001; Liu et al., 2009; Skjerlie and Patiño Douce, 2002) of these phases in metabasite. The phase relations vary with bulk rock and mineral composition. For example, Lopez and Castro (2001) used an amphibolite as a starting material, while Skjerlie and Patiño Douce (2002) did experiments on zoisite eclogite and Liu et al. (2009) did the same on phengite eclogite. The bulk composition of the studied eclogites, being similar to starting materials in Skjerlie and Patiño Douce (2002), yielded a pseudosection with large discrepancies in the upper thermal limits of zoisite + melt (Fig. 10) compared to the experimental results. The upper thermal stability of zoisite in experiments and theoretical calculations differs by  $> 100$  °C (Skjerlie and Patiño

Douce, 2002; Vielzeuf and Schmidt, 2001) for specific mafic bulk compositions, indicating the need for further examination. Wei and Duan (2018) compared phase relations of melt and other phases for a mid-ocean ridge basalt (MORB)-based pseudosection with various experiments and showed that the stability fields are consistent for amphibole and epidote at suprasolidus; however, considerable discrepancies are present at subsolidus, which shows shrunken epidote and enlarged amphibole fields. Forshaw et al. (2019) attributed discrepancies between observed and predicted values in amphibole and clinopyroxene chemistry from high-temperature metabasite to incorrect element partitioning and substitution vectors by the models. The current thermodynamic dataset and solution models for metabasite needs further development to correctly model the relevant phase relations.

#### 8 Concluding summary

Zoisite eclogites from the Sanddal area of the NEGEP were partially melted at near-peak  $P$  and on the exhumation path. The mineral assemblage at peak  $P$  was garnet, omphacite, kyanite, zoisite, phengite, quartz and rutile. Isochemical phase equilibrium modeling of the melt-reintegrated rock composition, along with isopleths of Si-in-phengite and  $X_{\text{Na}}$ -in-clinopyroxene, yields peak- $P$  conditions of  $2.4 \pm 0.1$  GPa at  $830 \pm 30$  °C. Partial melting is indicated by microscopic and mesoscopic melt-related textures. Graphic amphibole-plagioclase intergrowths and small garnet neoblasts adjacent to anhedral zoisite and clinopyroxene with plagioclase cusps point to the principal reaction being zoisite + clinopyroxene = melt + garnet. Polymineralic inclusions of K-feldspar, albite and other phases with sharp offshoots into garnet hosts crystallized from melt derived from breakdown of phengite and paragonite previously enclosed in garnet. A small percentage of melt loss occurred, leading to formation of leucocratic veins within the eclogite pod and foliated eclogite at the rim. A pseudosection of a melt domain, along with garnet and plagioclase isopleths, yields a peak  $T$  of  $900 \pm 50$  °C at  $1.9 \pm 0.2$  GPa following peak  $P$ . Phase equilibrium modeling of the melt-reintegrated composition further corroborated the presence of paragonite on the prograde path and yielded peak conditions similar to the ones using the bulk rock. The eclogite reached an equilibrium condition of 1.3 GPa and 750 °C, determined by thermobarometry using amphibole and plagioclase formed on the retrograde path.

*Data availability.* Additional mineral chemistry will be provided upon request.

*Supplement.* The supplement related to this article is available online at: <https://doi.org/10.5194/ejm-32-405-2020-supplement>.

*Author contributions.* JAG collected the samples and secured major funding for the research. JAG, HJM and WTC designed the research project. WTC carried out detailed petrography, mineral chemistry, thermobarometry and phase equilibrium modeling. WTC prepared the manuscript with significant contributions from the other co-authors.

*Competing interests.* The authors declare that they have no conflict of interest.

*Acknowledgements.* The authors thank Thomas Theye for his help with the electron microprobe analysis and Simona Ferrando, Tom Foster, Chun-Jing Wei and Giselle Rebay for valuable discussions and comments on an earlier version of the paper. We also wish to thank Aphrodite Indares and an anonymous reviewer for constructive comments, and Chiara Groppo and Elisabetta Rampone for editorial handling and comments that have significantly improved this paper. Publication of the study was supported by the GPMR research grant (GPMR201818) to Wentao Cao. Wentao Cao appreciates the support of the T. Anne Cleary Dissertation Research Fellowship, Post-comprehensive Summer Research Fellowship, and Ballard and Seashore Dissertation Fellowship from the Graduate College, University of Iowa.

*Financial support.* This research has been supported by the National Science Foundation, Division of Earth Sciences (grant no. 1049433).

*Review statement.* This paper was edited by Chiara Groppo and reviewed by Aphrodite Indares, Chiara Groppo, and one anonymous referee.

## References

- Anderson, J. L. and Smith, D. R.: The effects of temperature and  $fO_2$  on the Al-in-hornblende barometer, *Am. Mineral.*, 80, 549–559, 1995.
- Bartoli, O.: Phase equilibria modelling of residual migmatites and granulites: an evaluation of the melt-reintegration approach, *J. Metamorph. Geol.*, 35, 919–942, <https://doi.org/10.1111/jmg.12261>, 2017.
- Brandelik, A.: CALCMIN – an EXCEL (TM) Visual Basic application for calculating mineral structural formulae from electron microprobe analyses, *Comput. Geosci.-Uk*, 35, 1540–1551, <https://doi.org/10.1016/j.cageo.2008.09.011>, 2009.
- Brey, G. P. and Köhler, T.: Geothermobarometry in four-phase lherzolites II: New thermobarometers, and practical assessment of existing thermobarometers, *J. Petrol.*, 31, 1353–1378, 1990.
- Brueckner, H. K., Gilotti, J. A., and Nutman, A. P.: Caledonian eclogite-facies metamorphism of Early Proterozoic protoliths from the North-East Greenland Eclogite Province, *Contrib. Mineral. Petrol.*, 130, 103–120, 1998.
- Cao, W., Gilotti, J. A., Massonne, H.-J., Ferrando, S., and Foster, C. T. J.: Partial melting due to breakdown of an epidote-group mineral during exhumation of ultrahigh-pressure eclogite: an example from the North-East Greenland Caledonides, *J. Metamorph. Geol.*, 37, 15–39, <https://doi.org/10.1111/JMG.12447>, 2019.
- Chen, D. L., Liu, L., Sun, Y., and Zhu, X. H.: The retrograde partial melting of the Xitieshan UHP eclogite from the North Qaidam, NW China, *Geochim. Cosmochim. Ac.*, 74, A167–A167, 2010.
- Chen, Y. X., Zheng, Y. F., Gao, X. Y., and Hu, Z.: Multiphase solid inclusions in zoisite-bearing eclogite: evidence for partial melting of ultrahigh-pressure metamorphic rocks during continental collision, *Lithos*, 200, 1–21, <https://doi.org/10.1016/j.lithos.2014.04.004>, 2014.
- Clemens, J. D.: Melting of the continental crust: fluid regimes, melting reactions, and source-rock fertility, *Evolution and differentiation of the continental crust*, edited by: Brown, M. and Rushmer, T., Cambridge University Press, Cambridge, UK, 2006.
- Connolly, J. A. D.: Computation of phase equilibria by linear programming: A tool for geodynamic modeling and its application to subduction zone decarbonation, *Earth Planet. Sci. Lett.*, 236, 524–541, <https://doi.org/10.1016/j.epsl.2005.04.033>, 2005.
- Deng, L.-P., Liu, Y.-C., Yang, Y., Groppo, C., Rolfo, F., and Gu, X.-F.: Anatexis of high-T eclogites in the Dabie orogen triggered by exhumation and post-orogenic collapse, *Eur. J. Mineral.*, 31, 889–903, <https://doi.org/10.1127/ejm/2019/0031-2884>, 2019.
- Ellis, D. J. and Green, D. H.: An experimental study of the effect of Ca upon garnet-clinopyroxene Fe-Mg exchange equilibria, *Contrib. Mineral. Petrol.*, 71, 13–22, <https://doi.org/10.1007/Bf00371878>, 1979.
- Elvevold, S. and Gilotti, J. A.: Pressure-temperature evolution of retrogressed kyanite eclogites, Weinschenk Island, North-East Greenland Caledonides, *Lithos*, 53, 127–147, [https://doi.org/10.1016/S0024-4937\(00\)00014-1](https://doi.org/10.1016/S0024-4937(00)00014-1), 2000.
- Fenn, P. M.: On the origin of graphic granite, *Am. Mineral.*, 71, 325–330, 1986.
- Ferrando, S., Frezzotti, M. L., Dallai, L., and Compagnoni, R.: Multiphase solid inclusions in UHP rocks (Su-Lu, China): Remnants of supercritical silicate-rich aqueous fluids released during continental subduction, *Chem. Geol.*, 223, 68–81, <https://doi.org/10.1016/j.chemgeo.2005.01.029>, 2005.
- Ferrero, S., Wunder, B., Walczak, K., O'Brien, P. J., and Ziemann, M. A.: Preserved near ultrahigh-pressure melt from continental crust subducted to mantle depths, *Geology*, 43, 447–450, <https://doi.org/10.1130/G36534.1>, 2015.
- Forshaw, J. B., Waters, D. J., Pattison, D. R., Palin, R. M., and Gopon, P.: A comparison of observed and thermodynamically predicted phase equilibria and mineral compositions in mafic granulites, *J. Metamorph. Geol.*, 37, 153–179, 2019.
- Fuhrman, M. L. and Lindsley, D. H.: Ternary-feldspar modeling and thermometry, *Am. Mineral.*, 73, 201–215, 1988.
- Gao, X. Y., Zheng, Y.-F., Chen, Y. X., and Hu, Z.: Composite carbonate and silicate multiphase solid inclusions in metamorphic garnet from ultrahigh-P eclogite in the Dabie orogen, *J. Metamorph. Geol.*, 32, 961–980, 2014.
- Gilotti, J. A.: Discovery of a medium-temperature eclogite province in the Caledonides of North-East Greenland, *Geology*, 21, 523–526, [https://doi.org/10.1130/0091-7613\(1993\)021<0523:Doamte>2.3.Co;2](https://doi.org/10.1130/0091-7613(1993)021<0523:Doamte>2.3.Co;2), 1993.

- Gilotti, J. A. and McClelland, W. C.: Characteristics of, and a tectonic model for, ultrahigh-pressure metamorphism in the overriding plate of the Caledonian Orogen, *Int. Geol. Rev.*, 49, 777–797, 2007.
- Gilotti, J. A. and McClelland, W. C.: Geochemical and geochronological evidence that the North-East Greenland ultrahigh-pressure terrane is Laurentian crust, *The J. Geol.*, 119, 439–456, <https://doi.org/10.1086/660867>, 2011.
- Gilotti, J. A. and Ravn, E. J. K.: First evidence for ultrahigh-pressure metamorphism in the North-East Greenland Caledonides, *Geology*, 30, 551–554, [https://doi.org/10.1130/0091-7613\(2002\)030<0551:Fefupm>2.0.Co;2](https://doi.org/10.1130/0091-7613(2002)030<0551:Fefupm>2.0.Co;2), 2002.
- Gilotti, J. A., Nutman, A. P., and Brueckner, H. K.: Devonian to Carboniferous collision in the Greenland Caledonides: U-Pb zircon and Sm-Nd ages of high-pressure and ultrahigh-pressure metamorphism, *Contrib. Mineral. Petrol.*, 148, 216–235, <https://doi.org/10.1007/s00410-004-0600-4>, 2004.
- Gilotti, J. A., Jones, K. A., and Elvevold, S.: Caledonian metamorphic patterns in Greenland, in: *The Greenland Caledonides: Evolution of the Northeast Margin of Laurentia*, edited by: Higgins, A. K., Gilotti, J. A., and Smith, M. P., *Geol. Soc. Am. Mem.*, 202, 201–225, 2008.
- Gilotti, J. A., McClelland, W. C., and Wooden, J. L.: Zircon captures exhumation of an ultrahigh-pressure terrane, North-East Greenland Caledonides, *Gondwana Res.*, 25, 235–256, <https://doi.org/10.1016/j.gr.2013.03.018>, 2014.
- Green, E. C. R., White, R. W., Diener, J. F. A., Powell, R., Holland, T. J. B., and Palin, R. M.: Activity-composition relations for the calculation of partial melting equilibria in metabasic rocks, *J. Metamorph. Geol.*, 34, 845–869, <https://doi.org/10.1111/jmg.12211>, 2016.
- Groppo, C., Rolfo, F., and Indares, A.: Partial Melting in the Higher Himalayan Crystallines of Eastern Nepal: the Effect of Decompression and Implications for the 'Channel Flow' Model, *J. Petrol.*, 53, 1057–1088, <https://doi.org/10.1093/petrology/egs009>, 2012.
- Hallett, B. W., McClelland, W. C., and Gilotti, J. A.: The timing of strike-slip deformation along the Storstrømmen shear zone, Greenland Caledonides: U-Pb zircon and titanite geochronology, *Geosci. Can.*, 41, 19–45, 2014.
- Harley, S. L. and Green, D. H.: Garnet ortho-pyroxene barometry for granulites and peridotites, *Nature*, 300, 697–701, <https://doi.org/10.1038/300697a0>, 1982.
- Hawthorne, F. C., Oberti, R., Harlow, G. E., Maresch, W. V., Martin, R. F., Schumacher, J. C., and Welch, M. D.: Nomenclature of the amphibole supergroup, *Am. Mineral.*, 97, 2031–2048, <https://doi.org/10.2138/am.2012.4276>, 2012.
- Hermann, J. and Green, D. H.: Experimental constraints on high pressure melting in subducted crust, *Earth Planet. Sci. Lett.*, 188, 149–168, [https://doi.org/10.1016/S0012-821x\(01\)00321-1](https://doi.org/10.1016/S0012-821x(01)00321-1), 2001.
- Hernández-Urbe, D., Hernández-Montenegro, J. D., Cone, K. A., and Palin, R. M.: Oceanic slab-top melting during subduction: Implications for trace-element recycling and adakite petrogenesis, *Geology*, 48, 216–220, 2020.
- Holdsworth, R. E. and Strachan, R. A.: Interlinked system of ductile strike slip and thrusting formed by Caledonian sinistral transpression in northeastern Greenland, *Geology*, 19, 510–513, 1991.
- Holland, T. J. B.: The reaction albite = jadeite + quartz determined experimentally in the range 600–1200 °C, *Am. Mineral.*, 65, 129–134, 1980.
- Holland, T. J. B. and Blundy, J.: Nonideal interactions in calcic amphiboles and their bearing on amphibole-plagioclase thermometry, *Contrib. Mineral. Petrol.*, 116, 433–447, <https://doi.org/10.1007/Bf00310910>, 1994.
- Holland, T. J. B. and Powell, R.: A Compensated-Redlich-Kwong (CORK) equation for volumes and fugacities of CO<sub>2</sub> and H<sub>2</sub>O in the range 1 bar to 50 kbar and 100–1600 °C, *Contrib. Mineral. Petrol.*, 109, 265–273, <https://doi.org/10.1007/Bf00306484>, 1991.
- Holland, T. J. B. and Powell, R.: An improved and extended internally consistent thermodynamic dataset for phases of petrological interest, involving a new equation of state for solids, *J. Metamorph. Geol.*, 29, 333–383, <https://doi.org/10.1111/j.1525-1314.2010.00923.x>, 2011.
- Holness, M. B. and Sawyer, E. W.: On the pseudomorphing of melt-filled pores during the crystallization of migmatites, *J. Petrol.*, 49, 1343–1363, <https://doi.org/10.1093/petrology/egn028>, 2008.
- Holness, M. B., Cesare, B., and Sawyer, E. W.: Melted rocks under the microscope: Microstructures and their interpretation, *Elements*, 7, 247–252, <https://doi.org/10.2113/gselements.7.4.247>, 2011.
- Huang, W. L. and Wyllie, P. J.: Melting relations of muscovite with quartz and sanidine in K<sub>2</sub>O-Al<sub>2</sub>O<sub>3</sub>-SiO<sub>2</sub>-H<sub>2</sub>O system to 30 kilobars and an outline of paragonite melting relations, *Am. J. Sci.*, 274, 378–395, 1974.
- Hull, J. and Gilotti, J.: The Germania Land deformation zone, North-East Greenland, *Rapport Grønlands Geologiske Undersøgelse*, 162, 113–127, 1994.
- Indares, A., White, R. W., and Powell, R.: Phase equilibria modelling of kyanite-bearing anatectic paragneisses from the central Grenville Province, *J. Metamorph. Geol.*, 26, 815–836, <https://doi.org/10.1111/j.1525-1314.2008.00788.x>, 2008.
- Kalsbeek, F., Thrane, K., Higgins, A. K., Jepsen, H. F., Leslie, A. G., Nutman, A. P., and Frei, R.: Polyorogenic history of the East Greenland Caledonides, in: *The Greenland Caledonides: Evolution of the Northeast Margin of Laurentia*, edited by: Higgins, A. K., Gilotti, J. A., and Smith, M. P., *The Geological Society of America Memoir* 202, 55–72, 2008.
- Kretz, R.: Symbols for rock-forming minerals, *Am. Mineral.*, 68, 277–279, 1983.
- Labrousse, L., Prouteau, G., and Ganzhorn, A. C.: Continental exhumation triggered by partial melting at ultrahigh pressure, *Geology*, 39, 1171–1174, <https://doi.org/10.1130/G32316.1>, 2011.
- Lang, H. M. and Gilotti, J. A.: Plagioclase replacement textures in partially eclogitised gabbros from the Sanddal mafic-ultramafic complex, Greenland Caledonides, *J. Metamorph. Geol.*, 19, 495–515, 2001.
- Lang, H. M. and Gilotti, J. A.: Partial melting of metapelites at ultrahigh-pressure conditions, Greenland Caledonides, *J. Meta. Geol.*, 25, 129–147, <https://doi.org/10.1111/j.1525-1314.2006.00687.x>, 2007.
- Lang, H. M. and Gilotti, J. A.: Modeling the exhumation path of partially melted ultrahigh-pressure metapelites, North-East Greenland Caledonides, *Lithos*, 226, 131–146, <https://doi.org/10.1016/j.lithos.2014.10.010>, 2015.

- Liebscher, A., Franz, G., Frei, D., and Dulski, P.: High-pressure melting of eclogite and the P-T-X history of tonalitic to trondhjemitic zoisite-pegmatites, Munchberg Massif, Germany, *J. Petrol.*, 48, 1001–1019, <https://doi.org/10.1093/petrology/egm008>, 2007.
- Liu, P., Zhang, J., Massonne, H.-J., and Jin, Z.: Polyphase solid-inclusions formed by interactions between infiltrating fluids and precursor minerals enclosed in garnet of UHP rocks from the Dabie Shan, China, *Am. Mineral.*, 103, 1663–1673, <https://doi.org/10.2138/am-2018-6395>, 2018.
- Liu, Q., Jin, Z., and Zhang, J.: An experimental study of dehydration melting of phengite-bearing eclogite at 1.5–3.0 GPa, *Chinese Sci. Bull.*, 54, 2090–2100, <https://doi.org/10.1007/s11434-009-0140-4>, 2009.
- Liu, Q., Hermann, J., and Zhang, J. F.: Polyphase inclusions in the Shuanghe UHP eclogites formed by subsolidus transformation and incipient melting during exhumation of deeply subducted crust, *Lithos*, 177, 91–109, <https://doi.org/10.1016/j.lithos.2013.06.010>, 2013.
- Liu, Y. C., Deng, L. P., Gu, X. F., Groppo, C., and Rolfo, F.: Application of Ti-in-zircon and Zr-in-rutile thermometers to constrain high-temperature metamorphism in eclogites from the Dabie orogen, central China, *Gondwana Res.*, 27, 410–423, <https://doi.org/10.1016/j.gr.2013.10.011>, 2015.
- Locock, A. J.: An Excel spreadsheet to classify chemical analyses of amphiboles following the IMA 2012 recommendations, *Comput. Geosci.-Uk*, 62, 1–11, <https://doi.org/10.1016/j.cageo.2013.09.011>, 2014.
- London, D. and Morgan, G. B.: The pegmatite puzzle, *Elements*, 8, 263–268, 2012.
- Lopez, S. and Castro, A.: Determination of the fluid-absent solidus and supersolidus phase relationships of MORB-derived amphibolites in the range 4–14 kbar, *Am. Mineral.*, 86, 1396–1403, 2001.
- Massonne, H.-J.: Pre-conference field trip: Erzgebirge (Ore Mountains), Germany and Czech Republic; German part of the Saxonian Erzgebirge, *Geolines*, 23, 29–59, 2011.
- Massonne, H.-J.: Constructing the pressure-temperature path of ultrahigh-pressure rocks, *Elements*, 9, 267–272, <https://doi.org/10.2113/gselements.9.4.267>, 2013.
- Massonne, H.-J. and Sobiech, M.: Paragonite: Why is it so rare in medium-temperature high-pressure rocks?, *Int. Geol. Rev.*, 49, 301–312, <https://doi.org/10.2747/0020-6814.49.4.301>, 2007.
- McClelland, W. C., Power, S. E., Gilotti, J. A., and Mazdab, F. K.: U-Pb SHRIMP geochronology and trace-element geochemistry of coesite-bearing zircons, North-East Greenland Caledonides, in: *Geol. S. Am. S.*, edited by: Hacker, B. R., McClelland, W. C., and Liou, J. G., The Geological Society of America Special Paper 403, Boulder, CO, 23–43, 2006.
- McClelland, W. C., Gilotti, J. A., Ramarao, T., Stemmerik, L., and Dalhoff, F.: Carboniferous basin in Holm Land records local exhumation of the North-East Greenland Caledonides: Implications for the detrital zircon signature of a collisional orogen, *Geosphere*, 12, 925–947, <https://doi.org/10.1130/ges01284.1>, 2016.
- Mottana, A., Rossi, G., Kracher, A., and Kurat, G.: Violan revisited: Mn-bearing omphacite and diopside, *Tschermaks mineralogische und petrographische Mitteilungen*, 26, 187–201, <https://doi.org/10.1007/bf01081845>, 1979.
- Nestola, F., Merli, M., Nimis, P., Parisatoo, M., Kopylova, M., De Stefano, A., Longo, M., Ziberna, L., and Manghni, M.: In situ analysis of garnet inclusion in diamond using single-crystal X-ray diffraction and X-ray micro-tomography, *Eur. J. Mineral.*, 24, 599–606, <https://doi.org/10.1127/0935-1221/2012/0024-2212>, 2012.
- Palin, R. M., White, R. W., and Green, E. C.: Partial melting of metabasic rocks and the generation of tonalitic–trondhjemitic–granodioritic (TTG) crust in the Archaean: Constraints from phase equilibrium modelling, *Precambrian Res.*, 287, 73–90, 2016a.
- Palin, R. M., White, R. W., Green, E. C., Diener, J. F., Powell, R., and Holland, T. J.: High-grade metamorphism and partial melting of basic and intermediate rocks, *J. Metamorph. Geol.*, 34, 871–892, 2016b.
- Perchuk, A. L., Burchard, M., Maresch, W. V., and Schertl, H. P.: Fluid-mediated modification of garnet interiors under ultrahigh-pressure conditions, *Terra Nova*, 17, 545–553, <https://doi.org/10.1111/j.1365-3121.2005.00647.x>, 2005.
- Perchuk, A. L., Burchard, M., Maresch, W. V., and Schertl, H. P.: Melting of hydrous and carbonate mineral inclusions in garnet host during ultrahigh pressure experiments, *Lithos*, 103, 25–45, <https://doi.org/10.1016/j.lithos.2007.09.008>, 2008.
- Phillips, M., Colville, A., and Ribbe, P.: The crystal structures of two oligoclases: A comparison with low and high albite, *Zeitschrift für Kristallographie-Crystalline Materials*, 133, 43–65, 1971.
- Powell, R. and Holland, T. J. B.: On thermobarometry, *J. Metamorph. Geol.*, 26, 155–179, <https://doi.org/10.1111/j.1525-1314.2007.00756.x>, 2008.
- Ravna, E. J. K. and Terry, M. P.: Geothermobarometry of UHP and HP eclogites and schists – an evaluation of equilibria among garnet-clinopyroxene-kyanite-phengite-coesite/quartz, *J. Metamorph. Geol.*, 22, 579–592, <https://doi.org/10.1111/j.1525-1314.2004.00534.x>, 2004.
- Rosenberg, C. and Handy, M.: Experimental deformation of partially melted granite revisited: implications for the continental crust, *J. Metamorph. Geol.*, 23, 19–28, 2005.
- Rubatto, D.: Zircon trace element geochemistry: partitioning with garnet and the link between U-Pb ages and metamorphism, *Chem. Geol.*, 184, 123–138, [https://doi.org/10.1016/S0009-2541\(01\)00355-2](https://doi.org/10.1016/S0009-2541(01)00355-2), 2002.
- Rudnick, R. L. and Gao, S.: 4.1 – Composition of the Continental Crust A2 – Holland, Heinrich D., in: *Treatise on Geochemistry (Second Edition)*, edited by: Turekian, K. K., Elsevier, Oxford, 1–51, 2014.
- Sartini-Rideout, C., Gilotti, J. A., and McClelland, W. C.: Geology and timing of dextral strike-slip shear zones in Danmarkshavn, North-East Greenland Caledonides, *Geol. Mag.*, 143, 431–446, <https://doi.org/10.1017/s0016756806001968>, 2006.
- Schmidt, M. and Poli, S.: Devolatilization During Subduction, in: *Treatise on Geochemistry (Second Edition)*, edited by: Holland, H. D. and Turekian, K. K., Elsevier, Oxford, 669–701, 2014.
- Skjerlie, K. P. and Patiño Douce, A. E.: The fluid-absent partial melting of a zoisite-bearing quartz eclogite from 1.0 to 3.2 GPa: Implications for melting in thickened continental crust and for subduction-zone processes, *J. Petrol.*, 43, 291–314, <https://doi.org/10.1093/petrology/43.2.291>, 2002.

- Stöckhert, B., Duyster, J., Trepmann, C., and Massonne, H.-J.: Microdiamond daughter crystals precipitated from supercritical CO<sub>2</sub> plus silicate fluids included in garnet, Erzgebirge, Germany, *Geology*, 29, 391–394, [https://doi.org/10.1130/0091-7613\(2001\)029<0391:Mdcdfs>2.0.Co;2](https://doi.org/10.1130/0091-7613(2001)029<0391:Mdcdfs>2.0.Co;2), 2001.
- Stöckhert, B., Trepmann, C. A., and Massonne, H.-J.: Decrepitated UHP fluid inclusions: about diverse phase assemblages and extreme decompression rates (Erzgebirge, Germany), *J. Metamorph. Geol.*, 27, 673–684, <https://doi.org/10.1111/j.1525-1314.2009.00835.x>, 2009.
- Tomkins, H. S., Powell, R., and Ellis, D. J.: The pressure dependence of the zirconium-in-rutile thermometer, *J. Metamorph. Geol.*, 25, 703–713, <https://doi.org/10.1111/j.1525-1314.2007.00724.x>, 2007.
- Tual, L., Möller, C., and Whitehouse, M.: Tracking the prograde P–T path of Precambrian eclogite using Ti-in-quartz and Zr-in-rutile geothermobarometry, *Contrib. Mineral. Petrol.*, 173, 56, 2018.
- Vielzeuf, D. and Schmidt, M. W.: Melting relations in hydrous systems revisited: application to metapelites, metagreywackes and metabasalts, *Contrib. Mineral. Petrol.*, 141, 251–267, 2001.
- Wade, J., Dyck, B., Palin, R. M., Moore, J. D. P., and Smye, A. J.: The divergent fates of primitive hydro-spheric water on Earth and Mars, *Nature*, 552, 391–394, <https://doi.org/10.1038/nature25031>, 2017.
- Wang, L., Kusky, T. M., Polat, A., Wang, S., Jiang, X., Zong, K., Wang, J., Deng, H., and Fu, J.: Partial melting of deeply subducted eclogite from the Sulu orogen in China, *Nat. Commun.*, 5, 1–11, <https://doi.org/10.1038/ncomms6604>, 2014.
- Watson, E. B., Wark, D. A., and Thomas, J. B.: Crystallization thermometers for zircon and rutile, *Contrib. Mineral. Petrol.*, 151, 413–433, <https://doi.org/10.1007/s00410-006-0068-5>, 2006.
- Wei, C. and Duan, Z.: Phase relations in metabasic rocks: constraints from the results of experiments, phase modelling and ACF analysis, Geological Society, London, Special Publications, 474, SP474.410, 2018.
- White, R. W., Powell, R., and Clarke, G. L.: The interpretation of reaction textures in Fe-rich metapelitic granulites of the Musgrave Block, central Australia: constraints from mineral equilibria calculations in the system K<sub>2</sub>O-FeO-MgO-Al<sub>2</sub>O<sub>3</sub>-SiO<sub>2</sub>-H<sub>2</sub>O-TiO<sub>2</sub>-Fe<sub>2</sub>O<sub>3</sub>, *J. Metamorph. Geol.*, 20, 41–55, 2002.
- White, R. W., Powell, R., Holland, T. J. B., Johnson, T. E., and Green, E. C. R.: New mineral activity-composition relations for thermodynamic calculations in metapelitic systems, *J. Metamorph. Geol.*, 32, 261–286, <https://doi.org/10.1111/jmg.12071>, 2014.
- Yakymchuk, C. and Brown, M.: Consequences of open-system melting in tectonics, *J. Geol. Soc.*, 171, 21–40, 2014.
- Zack, T., Moraes, R., and Kronz, A.: Temperature dependence of Zr in rutile: empirical calibration of a rutile thermometer, *Contrib. Mineral. Petrol.*, 148, 471–488, <https://doi.org/10.1007/s00410-004-0617-8>, 2004.